Technical University of Munich
Physics Department

Bachelor Thesis

Universal few-particle nonflow scaling in multiparticle azimuthal correlators

Author: Matthias Wulff

Supervisor: Dr. Ante Bilandzic

July 29, 2019

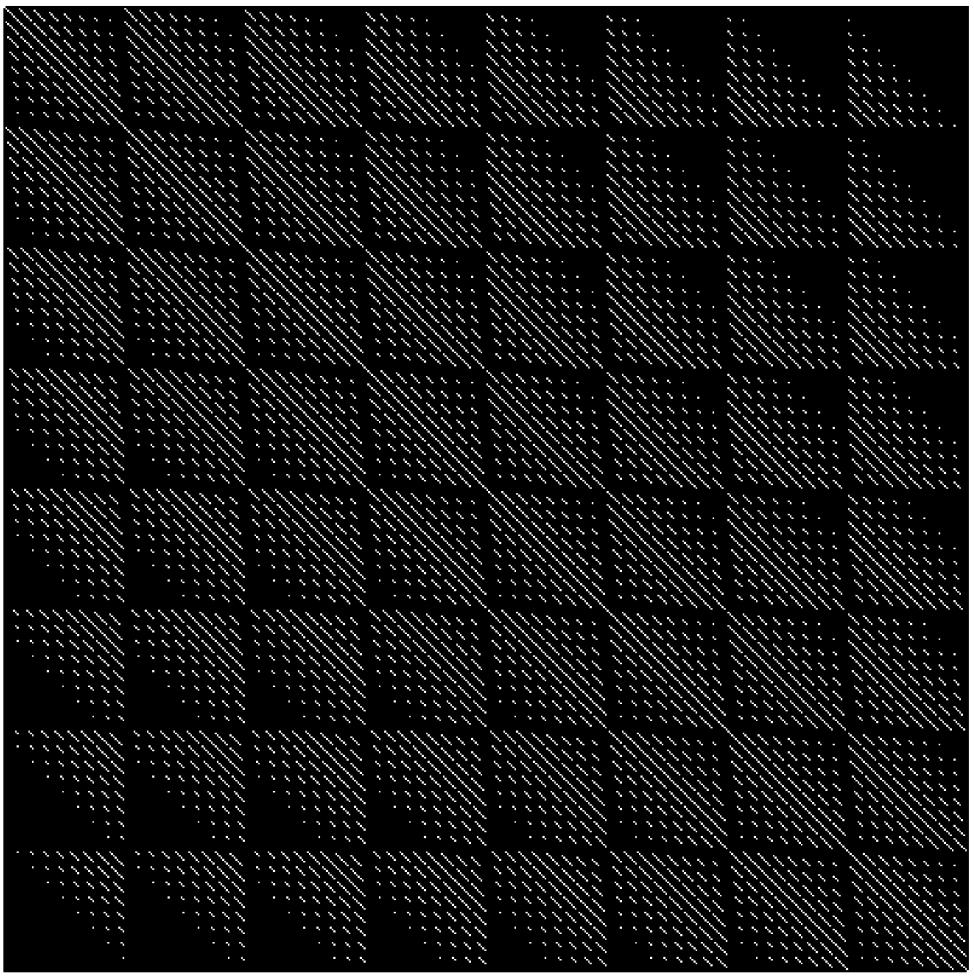

Abstract

In heavy-ion collisions extreme conditions arise which result in Quark-Gluon-Plasma (QGP). This QGP is then studied through anisotropic flow. This is the transport of an initial anisotropy in coordinate space, via the thermalized medium in which anisotropic pressure gradients develop, to an anisotropy in momentum space. The latter anisotropy can be observed by the detected particles produced in the collision. One uses a Fourier series to describe the distribution of the produced particles, and analysis its flow amplitudes through multiparticle correlations.

When analysing anisotropic flow by multiparticle azimuthal correlators, one is always confronted with systematic biases due to nonflow phenomena. Nonflow are all possible measured phenomena that are not a result of anisotropic flow. Due to the construction of multiparticle azimuthal correlators, nonflow is negligible with high multiplicities. On the other hand in smaller systems, lighter ion collisions such as p-p and p-A, the multiplicity is lower and nonflow effects cannot be neglected any more.

In this thesis, after giving a brief introduction, nonflow scaling of a few selected multiparticle azimuthal correlators are analysed. To do that, first flow and nonflow are removed by looking at the random walk of Q-vectors and how powers of them scale with the multiplicity. It is derived how any power/combination of Q-vectors scales in the random walk. The resulting findings are then applied to azimuthal correlators and Q-Cumulants containing them. Nonflow is then introduced by overcounting azimuthal angles (corresponding to track splitting) and it's nonflow scaling analytically found. This is then verified in a simple Monte Carlo study. It is then shown how the widely used probabilistic argument for leading-order nonflow scaling in k-particle azimuthal correlators deviates and even can fail at low multiplicities. Further a comparison on the nonflow scaling as a function of the multiplicity M between Q-Cumulants and the raw multiparticle correlators is done.

Contents

Chapter 1

Introduction

1.1 Quantum Chromodynamics (QCD)

The strong interaction, one of the four fundamental forces in nature, is described as a quantified field theory in Quantum Chromodynamics (QCD). QCD describes the interaction between quarks and gluons. Similar to the electric charge in Quantum Electrodynamics, particles can have a colour charge. In QCD quarks can carry a red, green or blue (and the corresponding anti-colors) as charge. By taking the color charge to define a local symmetry, QCD yields in a non-abelian gauge theory of the SU(3) gauge group. The requirement of local symmetry of "gauge invariance" results in the introduction of the gauge bosons of QCD - the gluons. Although Quarks only carry one unit of colour charge, gluons as "force carrier" additionally have a unit of anti-colour charge.

An important character of the strong force is *confinement*. If tried to isolate quarks and antiquarks the energy used to separate them is at some point favoured to be used to form new quarks and antiquarks from vacuum. Thus quarks and antiquarks can't be found isolated in nature but only confined in hadrons.

But because of the nature of the non-abelian group, gluon-gluon interactions are possible. This effects the vacuum-polarisation which is related to the phenomena of the running of the strong coupling. Connected to this is the *asymptotic freedom*. Due to the running of the strong coupling, the strong interaction gets very weak at high energies or small distances. Under these conditions quarks and gluons start to behave like free particles.

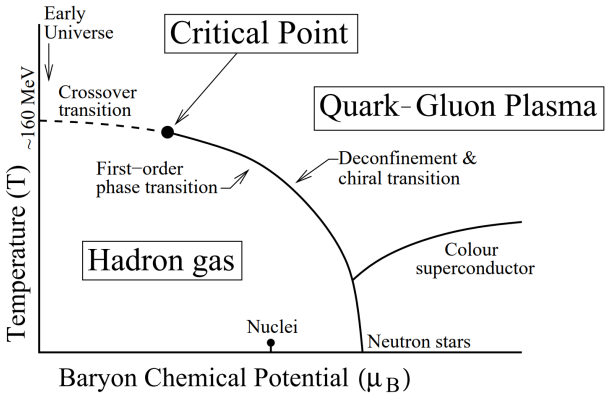

Figure 1.1: A schematic QCD phase diagram [9].

1.2 Quark-Gluon-Plasma (QGP)

Quark-Gluon-Plasma (QGP) is a state of nuclear matter directly related to the mentioned *asymptotic freedom*. It was realized that this implies a transition at high temperatures and high energy density to a phase of deconfined quarks and gluons [1].

Further it was shown with Lattice QCD calculations that the transition temperature from hadronic to deconfined state is achievable in the laboratory [2]. Scientists at European Organization for Nuclear Research (CERN) as well as at the Brookhaven National Laboratory's *Relativistic Heavy Ion Collider* (RHIC) soon announced they had created QGP [3, 4]. First it was thought QGP would behave simply like a weakly interacting gas, but early discoveries found that QGP behaves more like a perfect fluid with small shear viscosity to entropy density ratio (η/s) [5, 6]. The characteristic of this behaviour becomes important with new theoretical developments, as an example a lower bound on the shear viscosity over entropy density ratio $\eta/s > \hbar/4\pi k_B$ is given by using string theory methods [7]. Current experiments show that the created QGP is very close to this boundary (e.g. [8]).

Such a deconfined state of matter is believed to have existed a few microseconds after the Big Bang. By producing and studying properties of QGP in heavy-ion collisions essentially the same conditions of the distant past of our Universe are recreated at RHIC and the *Large Hadron Collider* (LHC). Our current understanding of strongly interacting matter can be qualitatively summarized in a QCD phase diagram in Fig. 1.1.

1.3 Heavy-Ion collisions

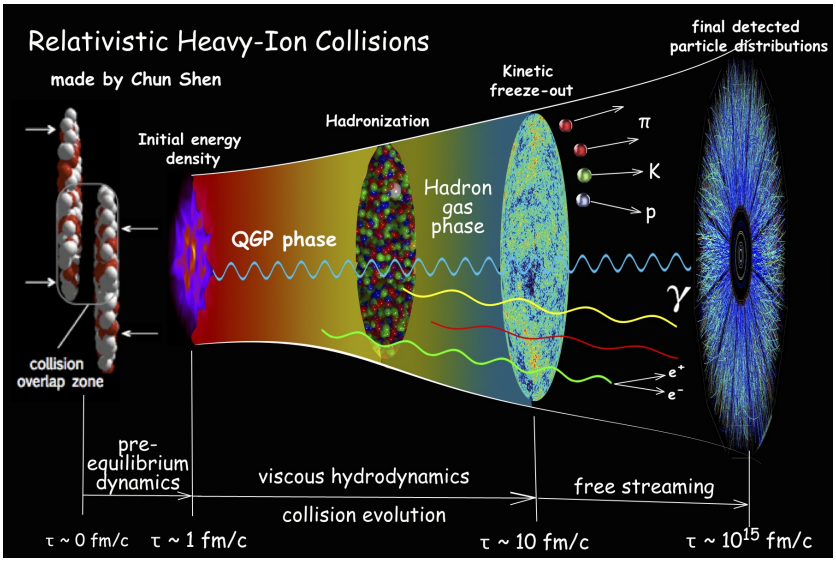

Figure 1.2: Space-time evolution of an ultra-relativistic heavy-ion collision [10].

To experimentally produce these extreme conditions under which QGP can exist, ultrarelativistic heavy-ion collisions is the way to go. From the centre of mass system each incoming nucleus is Lorentz-contracted and a coherent cloud of partons. Being nearly thermalized, the system evolves further under relativistic fluid dynamics, expanding, decreasing in energy density, cooling and hadronizing [9]. At first these hadrons have enough energy to scatter elastically as well as inelastically. When the energy per hadron does not allow any further inelastic processes, one speaks about the chemical freeze-out. As soon as all elastic processes stop, the thermal or kinetic freeze-out is reached. The produced hadrons now fly towards detectors, which are discussed in the next chapter. This evolution is illustrated in Fig. 1.2.

Heavy-ions are extended objects and hence the system created in peripheral collisions will be different than to the one created in head-on (central) collisions. Therefore, it is convenient to specify collisions by their *centrality* which is defined by the impact parameter b. The impact parameter describes the length of the vector connecting the two nuclei centres projected onto a plane transverse to the beam axis as can be seen in Fig. 1.3. There can also be seen that not all partons participate in the particle production. By looking at the *multiplicity* M (number of produced particles) distribution dN/dM, assuming the particle multiplicity M is monotonic as a function

of b, one can infer the centrality classes which are defined by binning the distribution as fractions of its total integral e.g. centrality 5%-10%:

$$\frac{\int_{\infty}^{N_{05}} \frac{dN}{dM} dM}{\int_{\infty}^{0} \frac{dN}{dM} dM} = 0.05 \tag{1.1}$$

and

$$\frac{\int_{\infty}^{N_{10}} \frac{dN}{dM} dM}{\int_{\infty}^{0} \frac{dN}{dM} dM} = 0.1. \tag{1.2}$$

High multiplicity events stem from central collisions and low multiplicity events from peripheral.

The *Glauber model* is a commonly used model in ultra-relativistic heavy-ion physics to calculate geometric quantities [11, 12]. First one takes two nuclei as the superposition of the constituent nucleons which are build from scratch from the Woods-Saxon distribution. Then one projects them into the transverse plane and determines if the nucleons collided. This occurs if their distance d to each other satisfies $d \leq \sqrt{\sigma_{\text{inel}}^{\text{NN}}/\pi}$; here $\sigma_{\text{inel}}^{\text{NN}}$ is the total inelastic nucleon-nucleon cross section. Now we can measure independently the number of participating nucleons (or *wounded* nucleons) $N_{\text{part}}(b)$ and the number of colliding nucleons $N_{\text{coll}}(b)$. We can also conveniently use Glauber model to calculate eccentricities in the initial state, which quantify the coordinate-space anisotropies and which are the starting point in anisotropic flow development. [13]

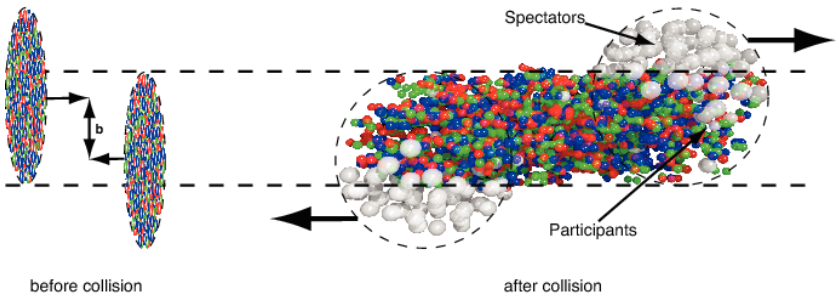

Figure 1.3: Two ultra-relativistic heavy-ions before colliding and shortly after collision [14].

Chapter 2

Experimental setup

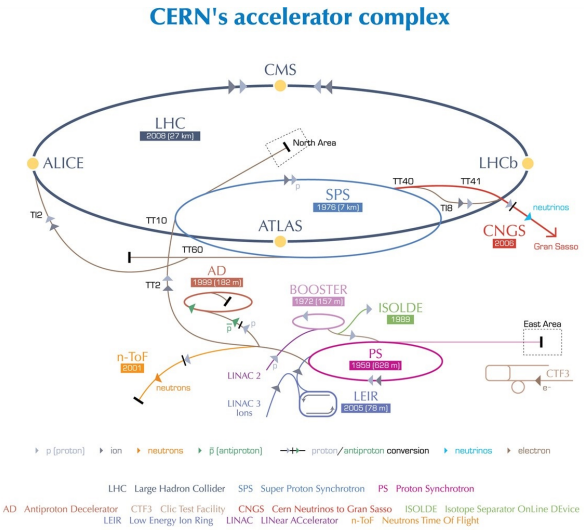

Figure 2.1: The CERN accelerator complex [15].

2.1 The Large Hadron Collider (LHC)

The LHC is located at CERN close to the French-Swiss border next to the Swiss city Geneva. It's the world's largest collider where thousands of scientists and engineers from all over the world produce 50 PB of data per year. The main storage ring of the synchrotron type accelerator is 100 meter beneath the ground and has a circumference of 27 km. After the 2015 upgrade the LHC achieved proton-proton (p-p) collisions with a centre of mass energy of up to $\sqrt{s} = 13$ TeV and lead-lead (Pb-Pb) collisions up to $\sqrt{s_{NN}} = 5.02$ TeV per nucleon pair. It will eventually achieve $\sqrt{s} = 14$ TeV for p-p and

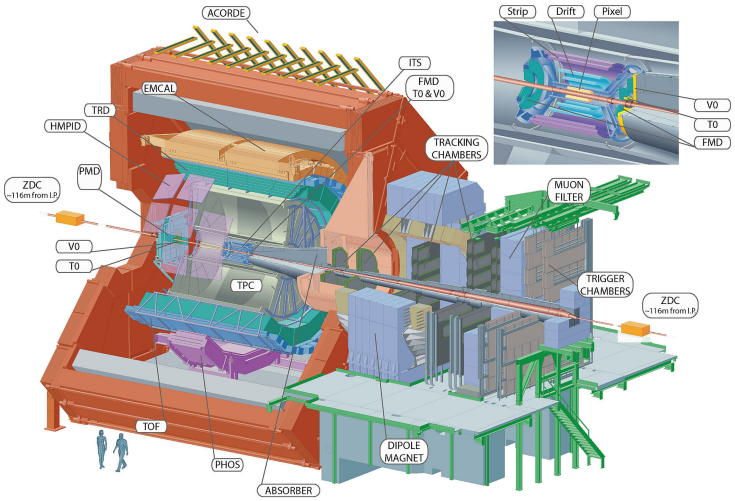

Figure 2.2: ALICE depicted in it's inner detectors [19].

$\sqrt{s_{NN}} = 5.52$ TeV per nucleon pair in Pb-Pb. To achieve these p-p energies the LHC accelerates 1.1×10^{11} protons as a bunch, with 2808 bunches per beam seperated by 25 ns, to 99.9999991% of the speed of light, meaning circling 11,245 times per second the ring, and colliding. This results in a design luminosity of 10^{34} cm^{-2}s^{-1} and $\approx$ 600 million p-p collsions per second. [16]

As illustrated in Fig. 2.1 there are four main experiments located around the LHC ring: *A Large Ion Collider Experiment* (ALICE), *A Toroidal LHS Apparatus* (ATLAS), *Compact Muon Solenoid* (CMS) and the *Large Hadron Collider beauty* (LHCb). ATLAS's and CMS's general purpose is to find new particles as they did with the Higgs [17, 18], LHCb is focused on bottom-quark physics in the forward regions and the study of matter-antimatter asymmetry in Universe. ALICE is the only dedicated heavy-ion experiment and is discussed in the following section.

2.2 ALICE

The ALICE detector is located in Saint-Genis-Pouilly, France. The goal of ALICE is to investigate the strongly interacting QCD matter created in the ultra-relativistic heavy-ion collisions, QGP being one main field of interest. The ALICE detector, shown in Fig. 2.2, is $16 \times 16 \times 26$ m^3 big, weighs 10 000 t and has 18 subdetectors, as they were used directly in the experimental part of this project. At three of them we will have a closer look. These achieve high- momentum resolution, good particle identification (PID) and track reconstruction over a broad range of momentum, although having to

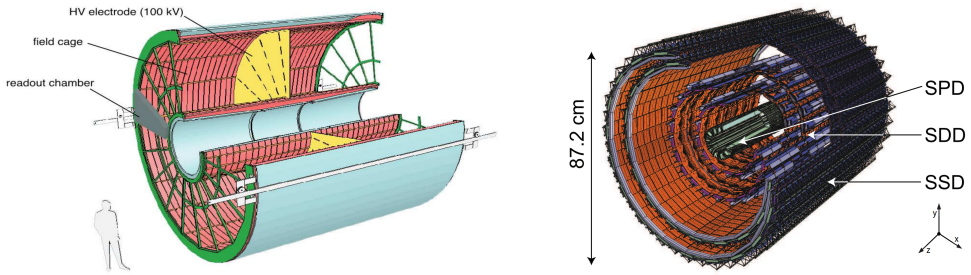

(a) (b)

Figure 2.3: ALICE's Time Projection Chamber (TPC) in (a) and ALICE's Inner Tracking System (ITS) in (b) [13, 21].

deal with extreme particle multiplicities in the heavy-ion collisions. [20]

Starting at the centre in Fig. 2.2 of the ALICE detector, first is the *Inner Tracking System* (ITS) with six layers of high-resolution *Silicon Pixel Detectos* (SPD), *Silicon Drift Detectors* (SDD) and *Silicon Strip Detectors* (SSD), then follows a cylindrical *Time Projection Chamber* (TPC) and three particle identification arrays consisting of *Time-of-Flight* (TOF), Ring Imaging Cherenkov and *Transition Radiation Detectors* (TRD) followed by two *Electromagnetic Calorimeters* (Photon Spectrometer - PHOS and EMCal).

2.2.1 Time Projection Chamber (TPC)

The TPC detector [20, 22] is one of the biggest and most important tracking detectors. As can be seen in Fig. 2.3a it is cylindrical and separated into two parts with a cathode in the middle. It has a longitudinal length of 5 m, with an innermost radius of 85 cm and outer radius of 250 cm. It is filled with 90 m^3 of gas (90% Ne, 10% CO_2). When a charged particle traverses, the gas is being ionized and the liberated electrons drift towards the end plates where they get detected by *Multi- Wire Proportional Chambers* (MWPC). Now the drift time is used to determine the z-coordinate, while the r- and φ coordinates are directly obtained by the MWPC's. The drift time of $\approx$ 90 μs is the limiting factor for the luminosity ALICE can cope with. The TPC is capable of detecting the particles in the transverse momentum range of $0.1 < p_T < 100$ GeV/c, with a transverse momentum resolution of about 6% for $p_T \leq 20$ GeV/c in central Pb-Pb collisions, and about 4.5% for $p_T \leq 20$ GeV/c in p-p collisions. The track finding efficiency saturates at about 90% for $p_T > 1$ GeV/c and the azimuthal resolution is about $\Delta\varphi = 0.7$ mrad for the whole p_T range. Although the TPC covers full azimuth acceptance, a dead zone between the neighbouring sectors (there are 16 sectors altogether)

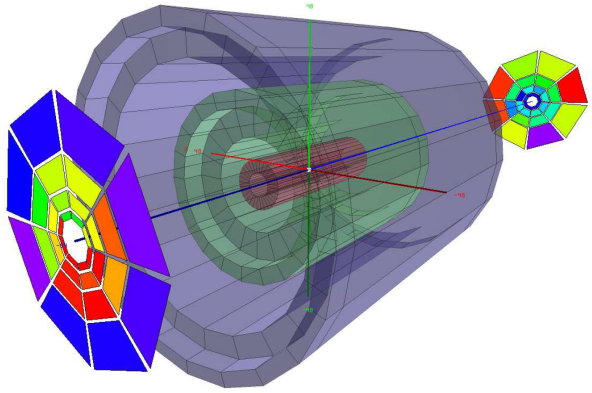

Figure 2.4: VZERO detectors on both sides of ITS. [13]

exist, essentially limiting the efficiency. Furthermore it has a pseudorapidity coverage of $|\eta| \leq 0.9$ for tracks traversing the whole radial length.

Although the TPS's main purpose is tracking, it can also be used for particle identification by dE/dx analysis and centrality estimations. Overall the uniform azimuthal coverage of the TPC makes it an ideal detector and for flow studies, since non-uniform acceptance would result in systematic biases which otherwise one has to correct for.

2.2.2 Inner Tracking System (ITS)

The ALICE Inner Tracking System [20, 23, 24] is shown in Fig. 2.3b. It consists of 6 silicon layers, with three groups of two layers forming three distinct detectors. The innermost two silicon layers are composed of *Silicon Pixel Detector* (SPD), the third and fourth layer consists of *Silicon Drift Detector* (SDD), and the outermost two layers are based on *Silicon Strip Detector* (SSD). The ITS covers a pseudorapidity range of $|\eta| \leq 0.9$ for interaction vertices within 5 cm along the beam, although the first SPD layer has a coverage of $|\eta| \leq 2.0$. Combined, the layers of the ITS can locate the primary vertex with a resolution better than 100 μm. It can also give information about low p_{T} particles ($\leq 100\mathrm{MeV}/c$), which do not reach the TPC. If the particle traversed all 6 layers, a track can be fitted and charge and momentum of the particle can be found. Furthermore dE/dx analysis is possible in the 4 outer layers.

2.2.3 VZERO

The VZERO detector [20, 25] seen in Fig. 2.4 consists of two separate arrays of scintillator counters, V0A and V0C, placed on different sides of the central barrel detectors along the beam line. V0A and V0C are placed asymmetrically with respect to the interaction point. Because of this asymmetry, V0A and V0C have different pseudorapidity coverages. V0A covers a pseudorapidity range of $2.8 < \eta < 5.1$, while V0C covers $-3.7 < \eta < -1.7$. Each set of VZERO arrays contain 32 elementary counters arranged in 4 rings and 8 sectors of 45° each.

The VZERO detector serves various purposes such as centrality determination. There it has a resolution of about 0.5% centrality bin width in the most central collisions, and a resolution still better than 2% centrality bin width for peripheral collisions. [24]

Chapter 3

Anisotropic flow

In Fig. 3.1 the collision of two heavy-ions can be seen in the transverse plane, which is perpendicular to the beam axis z. The properties of QGP in ultra-relativistic heavy-ion collisions are studied by azimuthal angle φ anisotropies enabled by anisotropic flow. Anisotropic flow is the transition of the anisotropy from the initial coordinate space, due to the initial collision geometry, into the final momentum space via the thermalized medium. The medium needs to be thermalized, so that anisotropic pressure gradients can develop and through flow, transfer the anisotropy from the initial spatial state into the momentum space of the final state which are experimentally accessible via the produced particles and their azimuthal angle φ. The distributions of the produced particles are described by a Fourier series:

$$f(\varphi) \propto \frac{1}{2\pi}[1 + 2\sum_{n=1}^{\infty} v_n \cos\left(n[\varphi - \Psi_n]\right)], \tag{3.1}$$

in which v_n are *anisotropic flow amplitudes*, and Ψ_n the corresponding *symmetry planes*. Here v_1 is direct flow, v_2 is elliptic flow, v_3 is triangular flow etc. [28]

Since the initial anisotropy in coordinate space is due to the initial collision geometry, it depends on the centrality classes how strong flow is e.g. in the mid-central collisions elliptic flow v_2 is dominant, but in the most head on collisions all (lower) order harmonics are equally probable as all of them originate solely from fluctuations. This superposition can be seen in Fig. 3.2. [13]

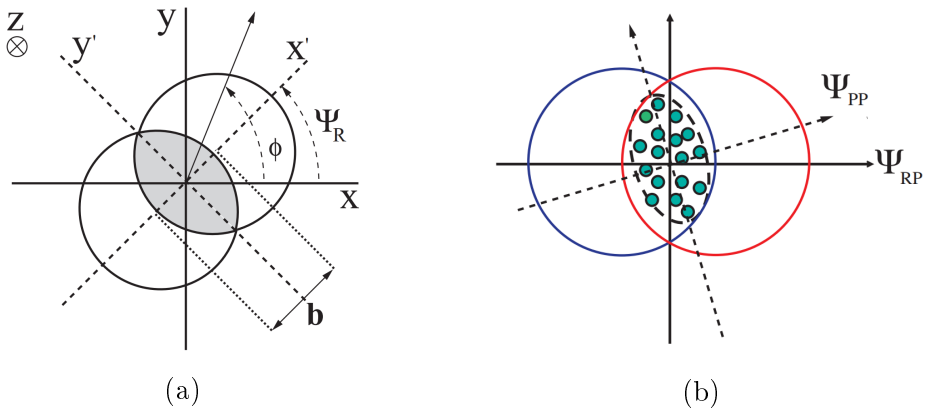

(a) (b)

Figure 3.1: Schematic view of a non-central nucleus-nucleus collision drawn in the transverse plane perpendicular to the beam axis z showing in (a) together with the reaction plane Ψ_{R}. The difference between a reaction plane and the participant plane Ψ_{PP} can be seen in (b) [26, 27].

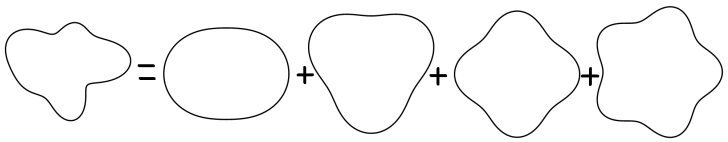

Figure 3.2: Superposition of different flow amplitudes.

These anisotropic flow amplitudes can now be connected to transport coefficients of QGP (e.g. in [29]). As an example a large anisotropic flow goes hand in hand with a small shear viscosity.

An important assumption in distinguishing flow correlations from other sources of correlations is the *flow principle*. It says that the correlations among all particles produced is solely induced by the correlation of each single particle to the collision geometry if the only source of correlations is anisotropic flow. Thus whether or not particles are emitted simultaneously or one by one, their trajectories are the same. [13] This results in the statistical independence

$$f(\varphi_1, ..., \varphi_i) = f(\varphi_1) \cdots f(\varphi_i). \tag{3.2}$$

To observe flow, different observables with different sensitivities are used. One can directly measure the flow amplitudes $v_1, v_2, v_3, ...$ or correlations between harmonics (e.g. $\langle v_m^2 v_n^2 \rangle - \langle v_m^2 \rangle \langle v_n^2 \rangle$) as well as symmetry plane correlations.

Chapter 4

Q-Cumulants and multiparticle correlations

Generally, the azimuthal angles φ_i, the flow amplitudes v_n and the symmetry planes Ψ_n are analytically connected by [30]:

$$\langle e^{i(n_1\varphi_1+\cdots+n_m\varphi_m)}\rangle = v_{n_1}\cdots v_{n_m}e^{i(n_1\Psi_1+\cdots+n_m\Psi_{n_m})}. \tag{4.1}$$

Here the average $\langle ...\rangle$ goes over all tuples of m different azimuthal angles φ_i.

There is one necessity which results in the *isotropic condition*. It constrains the different harmonics $n \in \mathbb{Z}$:

$$\sum_i n_i = 0. \tag{4.2}$$

This *isotropic condition* has to be the case when one imagines a detector that is simply rotated along the beam-axis. The results should stay the same, so this rotation angle must cancel out.

The correlation techniques introduced in the following can always be connected via Eq. (4.1) to the flow amplitudes v_n^k. These different flow moments carry independent information about the underlying p.d.f. $f(v_n)$:

$$\langle v_n^k\rangle = \int v_n^k f(v_n)dv_n. \tag{4.3}$$

A priori it is not guaranteed that a p.d.f. $f(v_n)$ is uniquely determined by its moments $\langle v_n^k\rangle$. But this is the case if the Krein-Lin conditions are met.[1] [31]

[1] $K[f] \equiv \int_0^\infty \frac{-\ln f(x^2)}{1+x^2}dx \Rightarrow K[f] = \infty$ and $L(x) \equiv -\frac{xf'(x)}{f(x)} \Rightarrow \lim_{x\to\infty} L[x] = \infty$.

4.1 Correlation techniques

Since our data is cyclic, one has to be careful when analysing the azimuthal angles. For example if one calculates the average of two angles simply directly, e.g. 10° degree and 350°, one gets 180° instead of the actual average 0°. A simple solution is to move into the complex plane and look at the azimuthal angles as phase shifts. As a result one has to define Q-vectors and can now add angles for multiparticle correlations by multiplication.
Furthermore one has to exclude autocorrelations. This results in some implementation problems. If getting rid of them by simply using nested loops, the computation time simply blows up. Thus a different approach has to be taken. This autocorrelation problem can also be solved by using the Q-vectors.

4.1.1 Q-vectors

One of the most important objects in anisotropic flow analysis is the so-called Q-vector (or flow vector) evaluated in the harmonic n:

$$Q_n \equiv \sum_{i=1}^{M} e^{in\varphi_i}. \tag{4.4}$$

By using Q-vectors we can now immediately evaluate all particles and their correlation with a *single pass* over the data, for any harmonic n. The key point is, that all multi-particle azimuthal correlations can be expressed and evaluated analytically in terms of Q-vectors in different harmonics.

4.1.2 m-particle correlation

In the most general form the m-particle correlation, in harmonics $n_1, n_2, ..., n_m$, is [32]:

$$\begin{aligned} \langle m \rangle_{n_1,\ldots,n_m} &\equiv \left\langle e^{i(n_1\varphi_1+n_2\varphi_2+\cdots+n_m\varphi_m)} \right\rangle \\ &\equiv \frac{\sum\limits_{\substack{k_1,k_2,\ldots,k_m=1 \\ k_1\neq k_2\neq\ldots\neq k_m}}^{M} w_{k_1} w_{k_2} \cdots w_{k_m}\, e^{i(n_1\varphi_{k_1}+n_2\varphi_{k_2}+\cdots+n_m\varphi_{k_m})}}{\sum\limits_{\substack{k_1,k_2,\ldots,k_m=1 \\ k_1\neq k_2\neq\ldots\neq k_m}}^{M} w_{k_1} w_{k_2} \cdots w_{k_m}}. \end{aligned} \tag{4.5}$$

Analytically the m-particle correlation can be expressed in Q-vectors. But the higher the particle correlation, the more terms arise in order to remove the

autocorrelations. In fact the number of terms blow up rapidly, following the Bell sequence [32]. Thankfully the m-particle correlation can be expressed recursively and thus save coding lines and deliver an easy to compile code [32].

The weights in Eq. (4.5) can be used to remove any systematic biases originating from the detector. This will be demonstrated in a later following Toy Monte Carlo study. Generally w can depend on azimuthal angle, transverse momentum, pseudorapidity, etc.:

$$w = w(\varphi, p_T, \eta, ...). \tag{4.6}$$

If we only have unit weights we can rewrite Eq. (4.5) to [32]:

$$\langle m \rangle \equiv \underbrace{\langle \cos[n_1\varphi_1 + n_2\varphi_2 + ... + n_{m-1}\varphi_{m-1} + n_m\varphi_m] \rangle}_{\varphi_1 \neq \varphi_2 \neq ... \neq \varphi_{m-1} \neq \varphi_m} \tag{4.7}$$

$$= \frac{1}{\binom{M}{m} m!} \sum_{\substack{i,j,...,k,l=1 \\ (i \neq j \neq ... \neq k \neq l)}}^{M} e^{i(n_i\varphi_i + n_j\varphi_j + ... + n_k\varphi_k + n_l\varphi_l)}. \tag{4.8}$$

If we want to expand the m-particle correlation purely with Q-vectors, over which we can loop in a single pass, we first have to remove any autocorrelations. For instance the 2-particle correlation, without any weights, simply is:

$$\langle 2 \rangle \equiv \langle \cos\left(n(\varphi_1 - \varphi_2)\right) = \frac{1}{\binom{M}{2} 2!} \sum_{\substack{i,j=1 \\ (i \neq j)}}^{M} e^{in(\varphi_i - \varphi_j)} = \frac{1}{\binom{M}{2} 2!} \times \Big[|Q_n|^2 - M \Big]. \tag{4.9}$$

This is easy to see since we simply exclude the case $i = j$:

$$|Q_n|^2 = Q_n Q_n^* = \sum_{i,j=1}^{M} e^{in(\varphi_i - \varphi_j)} = \sum_{\substack{i,j=1 \\ (i \neq j)}}^{M} e^{in(\varphi_i - \varphi_j)} + M. \tag{4.10}$$

To leading order the statistical spread of a flow amplitude v, estimated with a m-particle correlator, in the data sample consisting of N events, where M is the multiplicity of an event, is given by [13]:

$$\sigma_v \propto \frac{1}{\sqrt{N}} \frac{1}{M^{m/2}} \frac{1}{v^{m-1}}. \tag{4.11}$$

In heavy-ion collisions with large v and M, this results in flow analyses with very high precision. On the other hand for small collision systems, with small v and M, these techniques are for some reason not reliable.

4.1.3 Toy Monte Carlo study

In this Toy Monte Carlo (MC) study, we remove any systematic bias from the detector, reproducing the results of [32].

A normalized Fourier-like function is used as probability density function (p.d.f.), $f(\varphi)$, to sample the azimuthal angles, parametrized with harmonics up to v_6 and reaction plane Ψ_{RP}:

$$f(\varphi) = \frac{1}{2\pi}(1 + 2v_1\cos(\varphi - \Psi_{RP}) + 2v_2\cos[2(\varphi - \Psi_{RP})] \tag{4.12}$$

$$+ 2v_3\cos[3(\varphi - \Psi_{RP})] + 2v_4\cos[4(\varphi - \Psi_{RP})] \tag{4.13}$$

$$+ 2v_5\cos[5(\varphi - \Psi_{RP})] + 2v_6\cos[6(\varphi - \Psi_{RP})]). \tag{4.14}$$

The reaction plane Ψ_{RP} fluctuates randomly per event and is sampled uniformly on the interval $[0, 2\pi)$. The input values of

$$v_n = 0.04 + n \cdot 0.01, \quad n = 1, 2, ..., 6, \tag{4.15}$$

are used as flow amplitudes.

Now we select one example from each isotropic correlator from Eq. (4.5) and Eq. (4.1):

$$\begin{aligned}
\langle 2\rangle &\equiv \langle 2\rangle_{-2,2} = v_2^2 = 3.6 \times 10^{-3},\\
\langle 3\rangle &\equiv \langle 3\rangle_{-5,-1,6} = v_1 v_5 v_6 = 4.5 \times 10^{-4},\\
\langle 4\rangle &\equiv \langle 4\rangle_{-3,-2,2,3} = v_2^2 v_3^2 = 1.764 \times 10^{-5},\\
\langle 5\rangle &\equiv \langle 5\rangle_{-5,-4,3,3,3} = v_3^3 v_4 v_5 = 2.4696 \times 10^{-6},\\
\langle 6\rangle &\equiv \langle 6\rangle_{-2,-2,-1,-1,3,3} = v_1^2 v_2^2 v_3^2 = 4.41 \times 10^{-8}.
\end{aligned}$$

We have three separate runs in our Toy MC study. First we run our simulation for the case of uniform azimuthal acceptance of our detector. In the second run we use a non-uniform azimuthal acceptance by reducing the particles registered in the azimuthal range of $60^\circ \leq \varphi < 120^\circ$ by 50%, resulting in the azimuthal acceptance distribution seen in Fig. 4.1. Now we calculate our particle correlators with no modification to the weights (setting them to 1).

In the third and last run we create weights to get rid of the systematic bias of the non-uniform azimuthal acceptance. To do this we invert the azimuthal acceptance, resulting in Fig. 4.2. Note that particle weights obtained from Fig. 4.2 do not have to be normalized, e.g. can be randomly displaced by a constant, because of the definition of the m-particle correlator in Eq. (4.5), which automatically enforces the normalization via the denominator term.

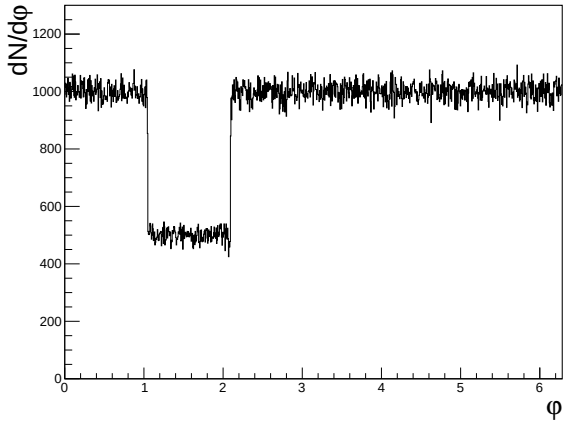

Figure 4.1: Non-uniform azimuthal acceptance, reducing the particles registered in the azimuthal range of $60° \leq \varphi < 120°$ by 50%.

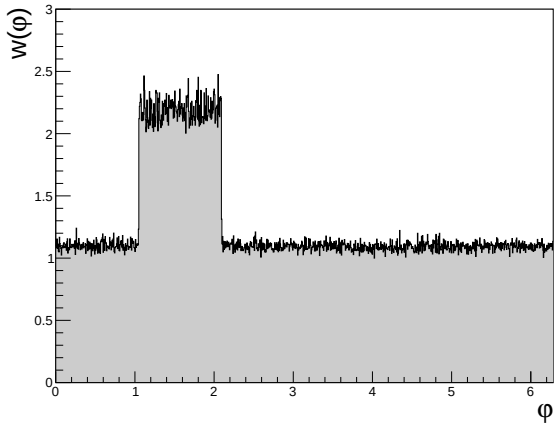

Figure 4.2: Weights derived from non-uniform azimuthal acceptance in Fig. 4.1

.

We can now use these weights and calculate the particle correlators again. In Fig. 4.3 we can see that the values now agree, within the errors, with the uniform azimuthal acceptance and the induced values of the particle correlators/corresponding harmonic flows.

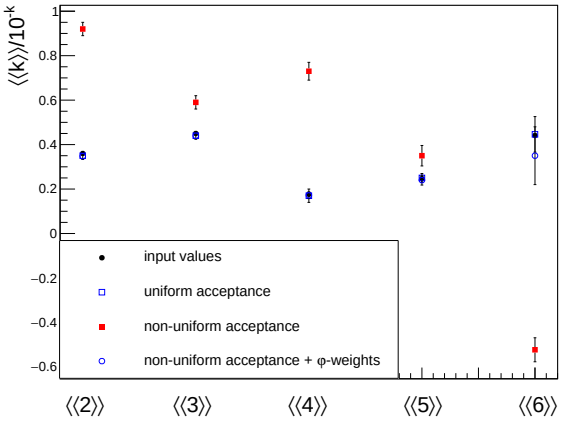

Figure 4.3: Multiparticle observables corrected for non-uniform acceptance using φ weights compared to input values and values for uniform acceptance.

4.2 Multiparticle cumulants

Cumulants can be used to describe p.d.f.'s and are an alternative to the moments of a distribution in a sense that for two p.d.f.'s whose moments are identical, also the cumulants will be and vice versa. They were originally introduced in order to be less sensitive to nonflow than the single multiparticle correlators in Eq. (4.5). [13, 33]

If two random variables X_1 and X_2 are statistically independent of each other, their joint p.d.f. $f(X_1, X_2)$ factorises

$$f(X_1, X_2) = f_{X_1}(X_1) \cdot f_{X_2}(X_2). \tag{4.16}$$

However if X_1 and X_2 aren't statistically independent, we can quantify this with a genuine 2-particle p.d.f. $f_c(X_1, X_2)$. Thus for a genuine 2-particle correlation we have the decomposition:

$$f(X_1, X_2) = f_{X_1}(X_1) \cdot f_{X_2}(X_2) + f_c(X_1, X_2), \tag{4.17}$$

which can be directly transfered to its expectation values

$$\langle X_1 X_2 \rangle = \langle X_1 \rangle \langle X_2 \rangle + \langle X_1 X_2 \rangle_c. \tag{4.18}$$

In practice we rarely know the exact form of p.d.f's in Eq. (4.17). However, we can use measured (sampled) values of the random variables X_1 and X_2 for the expectation values in Eq. (4.18). We are interested in the genuine 2-particle correlation from $f_c(X_1, X_2)$ and its contribution to $\langle X_1 X_2 \rangle$. Thus

we solve for $\langle X_1 X_2 \rangle_c$, which is by definition the 2-particle (or 2^{nd} order) cumulant[1]: [13]

$$\langle X_1 X_2 \rangle_c = \langle X_1 X_2 \rangle_c - \langle X_1 \rangle \langle X_2 \rangle. \tag{4.19}$$

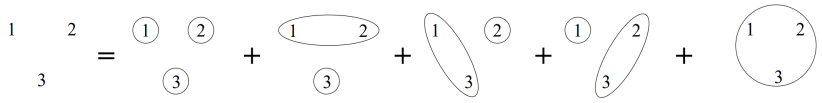

Figure 4.4: The decomposition of a 3^{rd} order cumulants [34]

This can be generalised to any order of multiparticle cumulants [35]. But the number of terms grow rapidly. As an example the decomposition of the 3-particle correlation in Fig. 4.4 can be seen. Mathematically written out this results in

$$\begin{aligned} \langle X_1 X_2 X_3 \rangle &= \langle X_1 \rangle \langle X_2 \rangle \langle X_3 \rangle & (4.20)\\ &+ \langle X_1 X_2 \rangle_c \langle X_3 \rangle + \langle X_1 X_3 \rangle_c \langle X_2 \rangle + \langle X_2 X_3 \rangle_c \langle X_1 \rangle & (4.21)\\ &+ \langle X_1 X_2 X_3 \rangle_c. & (4.22) \end{aligned}$$

Working now recursively from higher order of cumulants to lower order ones, we can now insert our result of the 2^{nd} order cumulant, in Eq. (4.18), and obtain:

$$\begin{aligned} \langle X_1 X_2 X_3 \rangle_c &= \langle X_1 \rangle \langle X_2 \rangle \langle X_3 \rangle & (4.23)\\ &- \langle X_1 X_2 \rangle \langle X_3 \rangle - \langle X_1 X_3 \rangle \langle X_2 \rangle - \langle X_2 X_3 \rangle \langle X_1 \rangle & (4.24)\\ &+ 2 \langle X_1 \rangle \langle X_2 \rangle \langle X_3 \rangle. & (4.25) \end{aligned}$$

It is important to note, that a cumulant $\langle X_i X_j \ldots \rangle_c$ is zero if the elements $X_i, X_j \ldots$ are divided in two or more groups which are statistically independent. This results in the fact that a cumulant is zero if one of the variables in it is independent of the others. Conversely, a cumulant is not zero if - and only if - the variables in it are statistically connected. [35]

We can apply this formalism to our random variables, the Q-vectors, in the harmonic n:

$$X_i = e^{i n_i \varphi_i}. \tag{4.26}$$

[1]Note that if X_1 and X_2 are statistically independent, $\langle X_1 X_2 \rangle = \langle X_1 \rangle \langle X_2 \rangle$, $\langle X_1 X_2 \rangle_c$ collapses to 0.

Therefore, the multiparticle cumulants read:

$$c_n\{1\} \equiv \langle\langle e^{in\varphi_1}\rangle\rangle, \tag{4.27}$$
$$c_n\{2\} \equiv \langle\langle e^{in(\varphi_1-\varphi_2)}\rangle\rangle - \langle\langle e^{in\varphi_1}\rangle\rangle\langle\langle e^{-in\varphi_2}\rangle\rangle, \tag{4.28}$$
$$c_n\{3\} \equiv \langle\langle e^{in(\varphi_1+\varphi_2-\varphi_3)}\rangle\rangle \tag{4.29}$$
$$- \langle\langle e^{in(\varphi_1+\varphi_2)}\rangle\rangle\langle\langle e^{-in\varphi_3}\rangle\rangle \tag{4.30}$$
$$- \langle\langle e^{in(\varphi_1-\varphi_3)}\rangle\rangle\langle\langle e^{in\varphi_2}\rangle\rangle \tag{4.31}$$
$$- \langle\langle e^{in(\varphi_2-\varphi_3)}\rangle\rangle\langle\langle e^{in\varphi_1}\rangle\rangle \tag{4.32}$$
$$+ 2\cdot\langle\langle e^{in\varphi_1}\rangle\rangle\langle\langle e^{in\varphi_2}\rangle\rangle\langle\langle e^{-in\varphi_3}\rangle\rangle, \tag{4.33}$$

and so on. The notation $c_n\{m\}$ means *cumulant estimated with m-particle correlations in harmonic n.*

4.2.1 Q-Cumulants

After the all-event average, due to the *isotropic condition* $\sum_i n_i = 0$ with all harmonics fixed as $n_i = n$, all odd particle number correlations m vanish. Using our unbiased m-particle correlation from Eq. (4.8) we can get [13]:

$$QC\{2\} \equiv \langle\langle 2\rangle\rangle, \tag{4.34}$$
$$QC\{4\} \equiv \langle\langle 4\rangle\rangle - 2\cdot\langle\langle 2\rangle\rangle^2, \tag{4.35}$$
$$QC\{6\} \equiv \langle\langle 6\rangle\rangle - 9\cdot\langle\langle 2\rangle\rangle\langle\langle 4\rangle\rangle + 12\cdot\langle\langle 2\rangle\rangle^3, \tag{4.36}$$
$$QC\{8\} \equiv \langle\langle 8\rangle\rangle - 16\cdot\langle\langle 6\rangle\rangle\langle\langle 2\rangle\rangle - 18\cdot\langle\langle 4\rangle\rangle^2 \tag{4.37}$$
$$+ 144\cdot\langle\langle 4\rangle\rangle\langle\langle 2\rangle\rangle^2 - 144\cdot\langle\langle 2\rangle\rangle^4. \tag{4.38}$$

These are the first few non-trivial isotropic cumulants evaluated in the same harmonics, when cumulants are defined as all-event averages.

4.2.2 Cumulants and flow

We could have used the connection to our flow amplitudes v_n in Eq. (4.1) to apply directly to $c_n\{2\}$ in Eq. (4.33). This results in

$$\langle\langle e^{in(\varphi_1-\varphi_2)}\rangle\rangle = v_n^2. \tag{4.39}$$

Thus we obtain

$$v_n\{2\} \equiv \sqrt{\langle\langle e^{in(\varphi_1-\varphi_2)}\rangle\rangle_c} = \sqrt{c_n\{2\}}, \tag{4.40}$$

and analogous for the 4-particle cumulant

$$v_n\{4\} \equiv \sqrt[4]{-\langle\langle e^{in(\varphi_1+\varphi_2-\varphi_3-\varphi_4)}\rangle\rangle_c} = \sqrt[4]{-c_n\{4\}}. \tag{4.41}$$

Flow Fluctuations

To derive cumulants, such as in Eq. (4.41), it was assumed that event-by-event fluctuations are negligible (e.g. $\langle v_n^2 \rangle^2 = \langle v_n^4 \rangle$). But $v_n\{2\}$ and $v_n\{4\}$ must be different in the presence of event-by-event fluctuations. To estimate the effect of such statistical flow fluctuations, one can use the Taylor series around the mean to expand to leading (second) order in the variance σ_{v_n}. [13]

This results in

$$v_n\{2\} \approx \langle v_n \rangle + \frac{\sigma_{v_n}^2}{2\langle v_n \rangle}, \tag{4.42}$$

$$v_n\{4\} \approx \langle v_n \rangle - \frac{\sigma_{v_n}^2}{2\langle v_n \rangle}. \tag{4.43}$$

The true mean value is always in-between these two estimates due to flow fluctuations.

4.2.3 Data selection and result

In this analysis, data from the ALICE detector recorded in 2010 (Pb–Pb collisions at a centre-of-mass energy of $\sqrt{s_{NN}}$= 2.76 TeV) from the runs 137161 and 138275 were taken for analysis.

First let's have a look at a few quality assurance (QA) plots to validate the dataset and track/event selection criteria. In Fig. 4.5) the azimuthal acceptance for central (0-5% centrality in Fig. 4.5a), midcentral(30-40% centrality in Fig. 4.5b) and peripheral(70-80% centrality in Fig. 4.5c) collisions can be seen. The resulting distribution looks clearly uniform and thus no additional weights have to be used for further analysis.

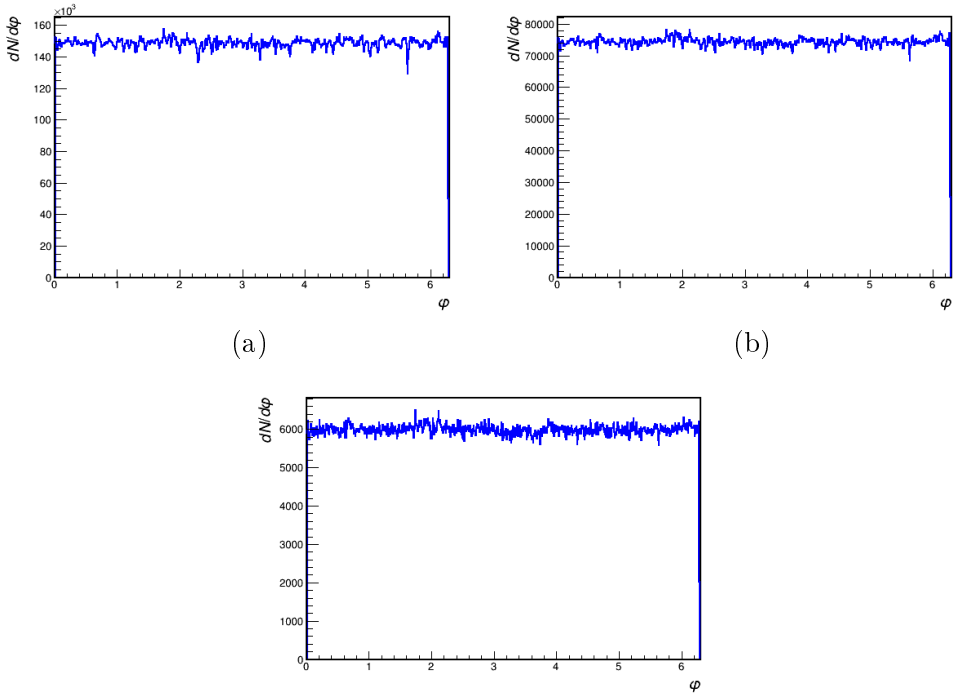

Figure 4.5: Distribution of azimuthal distribution for central (0-5% centrality in (a)), mid-central (30-40% centrality in (b)) and peripheral (70-80% centrality in (c)) collisions.

As we can see in Fig. 4.6 the multiplicity drops for central Fig. (4.6a), mid-central Fig. 4.6b and peripheral Fig. 4.6c collisions. In the case of the low multiplicities the statistical uncertainty gets bigger and bigger. In Fig. 4.7, we see the results of two and four-particle cumulants for elliptic flow v_2 and in Fig. 4.8 the results for the triangular flow v_3. Here we can clearly see that for the most central collisions v_2 and v_3 diminish since here the anisotropy in the coordinate space is rather low and thus the anisotropic flow. Further we see a maximal elliptic flow v_2 at about 50 % centrality. The decreasing value of v_2 is due to the lower multiplicity and therefore weaker flow, which goes hand in hand with higher uncertainties. But the 2-particle cumulant $v_2\{2\}$ deviates a bit from the 4-particle cumulant $v_2\{4\}$ since, as mentioned in the statistical spread of the m-particle correlation in section 4.1.2, it is more sensitive to nonlflow effects and flow fluctuations appear with a negative sign for $v_2\{4\}$ in Eq. (4.41). Nevertheless the obtained results are in agreement with the ALICE results of Elliptic flow of charged particles in Pb–Pb collisions at $\sqrt{s_{NN}}$= 2.76 TeV [36].

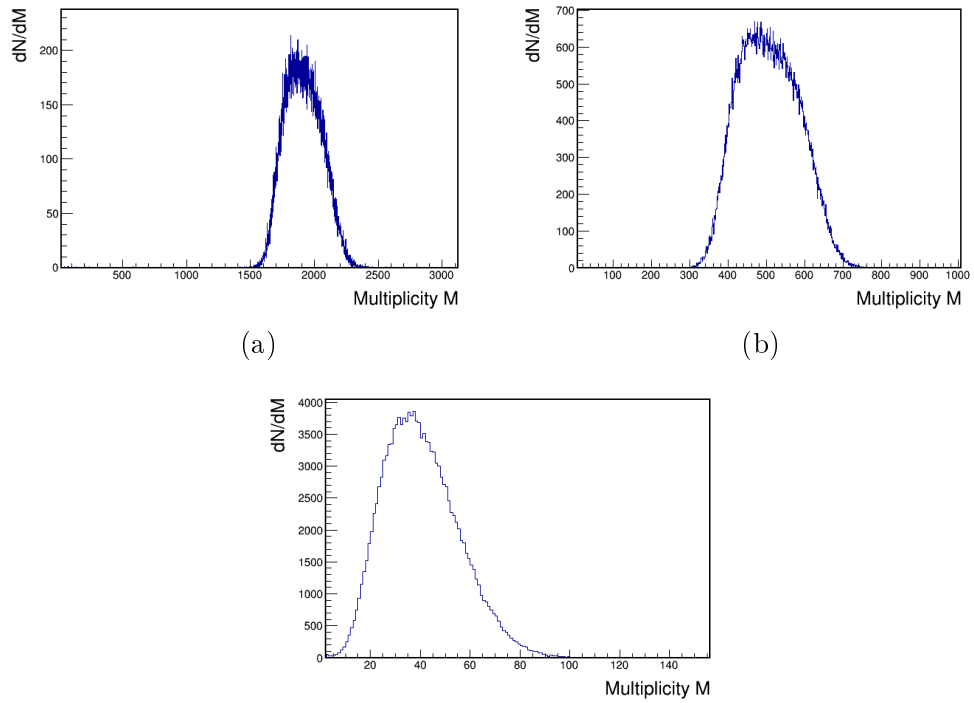

Figure 4.6: Distribution of multiplicity for central (0-5% centrality in (a)), mid-central (30-40% centrality in (b)) and peripheral (70-80% centrality in (c)) collisions.

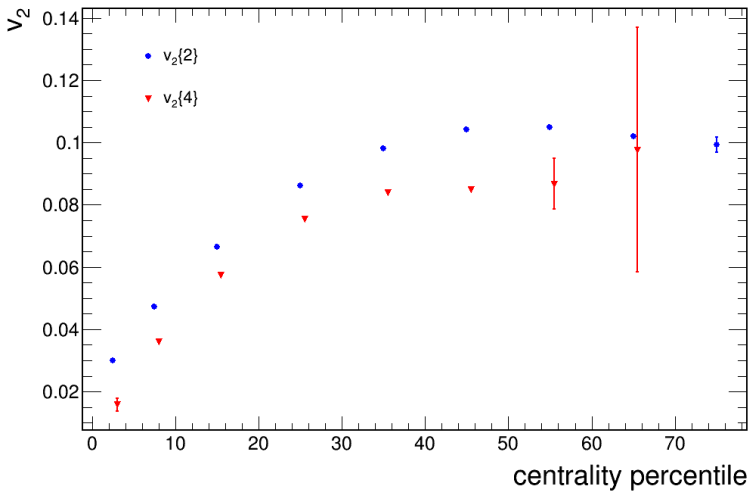

Figure 4.7: The elliptic flow v_2 in dependence of the centrality in Pb–Pb collisions at a centre-of-mass energy of $\sqrt{s_{NN}}$= 2.76 TeV recorded by the ALICE detector.

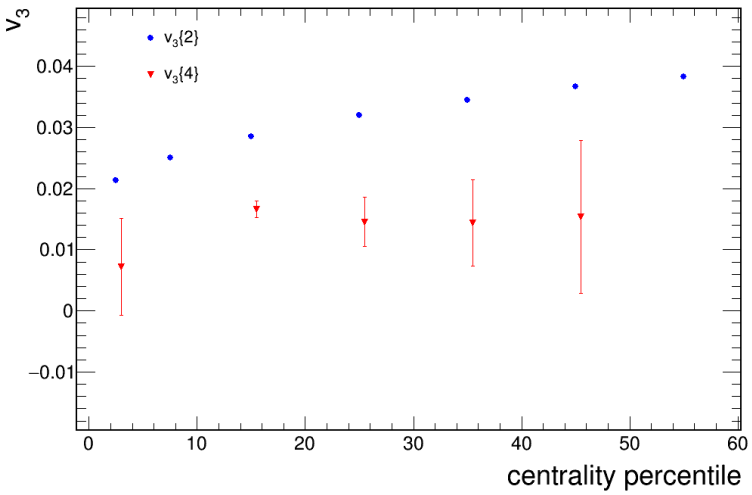

Figure 4.8: The triangular flow v_3 in dependence of the centrality in Pb–Pb collisions at a centre-of-mass energy of $\sqrt{s_{NN}}$= 2.76 TeV recorded by the ALICE detector.

Chapter 5

Nonflow scaling in azimuthal correlators

All other sources of contributions to azimuthal correlators, besides flow correlations, are classified as nonflow. These can be due to physical nonflow phenomena (resonance decays, jets, etc.), detector artefacts (track splitting in the reconstruction, etc.) or simply by the way we compute correlations when analysing flow (like autocorrelations).

The important difference is that flow is a collective effect and thus correlates all particles whereas nonflow is generally a correlation among few particles.

5.1 Nonflow scaling: the probabilistic argument

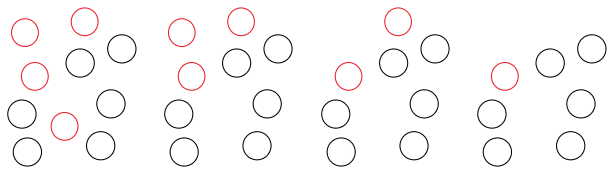

Figure 5.1: Illustration of the probabilistic argument.

There is a simple *probabilistic argument* resulting in a nonflow scaling in leading order of:

$$\delta_k \propto \frac{1}{M^{k-1}}. \tag{5.1}$$

Here k is the order chosen for the m-particle correlation. The mentioned scaling can easily be explained by an example illustrated in Fig. 5.1. If one chooses in this example to use a 4-particle correlation and some particles are correlated to each other due to nonflow (indicated in red), the question is what is the probability to choose only the particles that are correlated to each other due to this nonflow? After the first particle was selected there is one option less remaining etc., resulting in

$$\delta_4(nonflow) \approx \frac{3}{M-1}\frac{2}{M-2}\frac{1}{M-3} \approx \frac{1}{M^3}. \tag{5.2}$$

On the other hand flow is not effected by this probabilistic argument since it is a *collective phenomena*. It does not matter which particle we choose:

$$\delta_4(flow) \propto \frac{M-1}{M-1}\frac{M-2}{M-2}\frac{M-3}{M-3} \propto 1. \tag{5.3}$$

Usually the probabilistic argument is sufficient to neglect any nonflow implications in heavy-ion collisions, since the multiplicity is very high. It is one of the most important nonflow argument that is used in practice in the flow community. But if flow is being tried to be observed in small collisions systems like p-p or p-A, in which the multiplicity is lower, nonflow effects simply cannot be ignored any more. Thus a new understanding of nonflow scaling is absolutely necessary.

To get to the root of this problem one first has to understand how precisely the multiparticle correlators are affected by nonflow at low multiplicities, and whether in that regime nonflow contributions to azimuthal correlators exhibit any sort of universal scaling. To do this we set up Monte Carlo simulations, in which conditions are fully under control, and have a closer look at an induced nonflow scaling. This is done by first removing any flow and nonflow, and afterwards inducing nonflow by overcounting (corresponding to track splitting in the detector) resulting in an analytic expression of how nonflow should scale under these conditions.

5.2 Random walk - removal of flow and nonflow

To remove any flow or nonflow effects the random walk is used in order to inspect the genuine scaling of Q-vector with multiplicity, in the absence of any correlations. Since the sampled azimuthal angles are completely random, flow and nonflow can't be present [13]:

$$\langle 2 \rangle = \langle 3 \rangle = ... = \langle k \rangle = 0. \tag{5.4}$$

First we will set up some general rules for the random walk, and then calculate recursively the three cases $\langle 2\rangle = \langle 3\rangle = \langle 4\rangle = 0$ as done in [13]. After that, a new original procedure established in this project is used to get $\langle 6\rangle = \langle 8\rangle = 0$ directly. By doing it first recursively, we will get some intuition of what is actually happening and are then able to generalize our findings.

For further analysis we will need the 2-,3-,4-,6- and 8-particle correlations written in terms of Q-vectors and removed of any autocorrelation, these can be found in the Appendix A.1.

5.2.1 General rules for random walk

In order not to get confused later and to use results we obtained recursively, we have to establish some general rules.

- **Notation:** For the *average in the statistical limit of the random walk*, the obtained result will be distinguished by using a comment over the equal sign $\overset{stat.}{=}$ or expectation brackets $\langle ...\rangle$ (eg. Eq. (5.10) and Eq. (5.11)). One has to be careful to not raise $|Q_n|$ in $(\langle ...\rangle)$ to any power, since $\langle |Q_n|^2\rangle^2 \neq \langle |Q_n|^4\rangle$.

- **Angle additions have no impact:** It doesn't matter if we add any other additional value $\alpha \in \mathbb{R}$ to the azimuthal angle φ_i, since

$$Q_n = \sum_{j=1}^{M} e^{in(\varphi_j+\alpha)} = e^{in\alpha}\sum_{j=1}^{M} e^{i\varphi_j}, \tag{5.5}$$

  and the whole Q-vector expression has to follow the *isotropic condition*. Thus the additional angle cancel e.g. $|Q_n|^2 = Q_n Q_n^*$ and thus $e^{in\alpha}e^{-in\alpha} = 1$.[1] Thus as an example, the subtraction or addition of any angle α will have no effect on $|Q_n|^k$, with $k \in \mathbb{N}$.

- **factors in the exponent must be** $n \in \mathbb{Z}\setminus\{0\}$**:** This arises from[2]

$$\int_0^{2\pi} e^{in\varphi}d\varphi = \int_0^{2\pi} (\cos(n\varphi) + i\sin(n\varphi))d\varphi = \frac{\sin(2\pi n)}{n} + i\frac{2\sin^2(\pi n)}{n}, \tag{5.6}$$

  which has to be zero for the argument of the *average in the statistical limit of the random walk*.

[1] This would basically correspond to simply rotating the laboratory frame in which azimuthal angles are measured. But since all measurements have to be invariant under such rotation this rotation shift must cancel.

[2] Here the trigonometric relation $2\sin^2(x/2) = 1 - \cos(x)$ was used.

This will later be necessary to treat $\langle|Q_{2n}|^2\rangle$ with the results obtained from $\langle|Q_n|^2\rangle$.

- **Linear combination of azimuthal angles:** Furthermore the here appearing linear combination of randomly sampled azimuthal angles, are at first also assumed to be randomly distributed. For the linear combination the notation $\Delta\bar{\varphi}$ is used. Where any linear combination of azimuthal angles is meant, e.g.: $\Delta\bar{\varphi} = \varphi_1 + \varphi_2 - 2\cdot\varphi_3$, or more general $\Delta\bar{\varphi} = m_1\varphi_1 + ... + m_n\varphi_n$ ($n \in \mathbb{N}$ and $m_n \in \mathbb{Z}\setminus\{0\}$). There will be many of these additional terms, but since we will see that they have a small, almost negligible, contribution in the statistical limit let's simply write $\mathcal{O}(e^{i\Delta\bar{\varphi}})$ for them. If $\Delta\bar{\varphi}$ is randomly distributed $\langle\mathcal{O}(e^{i\Delta\bar{\varphi}})\rangle$ will disappear. This is derived in Appendix B.1.1.

  Notice one important thing: One has to be careful that the amount of i linear angles added doesn't get too big. This would result in further non trivial behaviour, because the *central limit theorem* would have the result that $\Delta\bar{\varphi}$ follows a normal distribution. As a result the argument in Appendix B.1.1 doesn't hold and $\langle\mathcal{O}(e^{i\Delta\bar{\varphi}})\rangle \neq 0$ is the case.
  Although the *central limit theorem* has a weak-convergence we will still see minor effects. But these can be estimated as shown in Appendix B.1.2. On the other hand, for $|Q_n|^k$ the linear combined azimuthal angles φ_i are maximal k.

Let's start with our first case of the random walk for $\langle 2\rangle$ and work recursively.

Case: $\langle 2\rangle = 0$

Starting from Eq. (5.4) it directly follows for the 2-particle correlation, Eq. (A.1), that:

$$\langle 2\rangle = 0 = \frac{|Q_n|^2 - M}{M(M-1)} \;\Leftrightarrow\; |Q_n|^2 = M. \tag{5.7}$$

This can be interpreted as the distance travelled, on average, in the complex plane via random walk from the origin. As an example a possible random walk can be seen in the quick sketch in Fig. 5.2a or for 500 steps in Fig. 5.2b.

(a) Q-vector walk (b) 500 steps

Figure 5.2: The random walk of a Q-vector in (a), and 500 random steps in (b)

By doing M steps in the complex plane it is well known that the average distance travelled is $\sqrt{M}$. So the result in Eq. (5.7) has some straight forward intuition to it. But actually carrying out the complete calculation with the Q-vector in Eq. (5.7) one gets a different result:

$$|Q_n|^2 = Q_n Q_n^* = \sum_{i=1}^{M} e^{in\varphi_i} \sum_{j=1}^{M} e^{in\varphi_j} \tag{5.8}$$

$$= \sum_{i,j=1}^{M} e^{in(\varphi_i - \varphi_j)} \tag{5.9}$$

$$= \underbrace{M}_{from\ i=j} + \sum_{\substack{i,j=1 \\ (i \neq j)}}^{M} e^{in(\varphi_i - \varphi_j)} \tag{5.10}$$

But since φ_i is sampled randomly from a uniform distribution between $[0, 2\pi)$, the last part disappears if $n \in \mathbb{Z}$ as can be seen in Eq. (5.6).

In order to not get confused with the actual Q-vector, in Eq. (5.10), and its average result in the statistical limit of the random walk, Eq.(5.11), let's write instead:

$$|Q_n|^2 \overset{stat.}{=} \langle |Q_n|^2 \rangle = M. \tag{5.11}$$

Case: $\langle 3 \rangle = 0$

From Eq. (5.4) the case of the 3-particle correlation, Eq. (A.2), leads to:

$$\langle 3 \rangle = 0 = \frac{\Re[Q_{2n}Q_n^*Q_n^*] - 2|Q_n|^2 - |Q_{2n}|^2 + 2M}{M(M-1)(M-2)} \tag{5.12}$$

$$\Leftrightarrow \tag{5.13}$$

$$\Re[Q_{2n}Q_n^*Q_n^*] = 2 \cdot \underbrace{|Q_n|^2}_{recursively\ Eq.(5.11)} + \underbrace{|Q_{2n}|^2}_{recursively\ Eq.(5.11)} - 2M \tag{5.14}$$

$$\Rightarrow \tag{5.15}$$

$$\Re[Q_{2n}Q_n^*Q_n^*] \overset{stat.}{=} 2M + M - 2M = M. \tag{5.16}$$

Now the obtained result in Eq. (5.16) is somewhat surprisingly equivalent to Eq. (5.11). But of course:

$$\Re[Q_{2n}Q_n^*Q_n^*] \neq |Q_n|^4. \tag{5.17}$$

One sees that there appear additional Q-vectors, which can be rewritten but nontheless not get rid off. But we assume that linear combinations of azimuthal angles are equally uniformly random. Thus in the average each $\langle e^{i\Delta\bar{\varphi}} \rangle$ is simply 0. The only terms remaining are those were $i = j = k$. The diagonal of the $i \times j \times k$ cube. We will elaborate on this later. Let's rewrite this generally with the $\Delta\bar{\varphi}$ notation:

$$\Re[Q_{2n}Q_n^*Q_n^*] = \Re[\sum_{i,j,k=1}^{M} e^{in(2\varphi_i - \varphi_j - \varphi_k)}] \tag{5.18}$$

$$= \frac{1}{2}[\sum_{i,j,k=1}^{M} e^{in(2\varphi_i - \varphi_j - \varphi_k)} + \sum_{i,j,k=1}^{M} e^{-in(2\varphi_i - \varphi_j - \varphi_k)}] \tag{5.19}$$

$$= \frac{1}{2}[2M + \underbrace{\mathcal{O}(e^{i\Delta\bar{\varphi}})}_{\langle e^{i\Delta\bar{\varphi}} \rangle = 0}] \tag{5.20}$$

Thus as average in the statistical limit we get:

$$\langle \Re[Q_{2n}Q_n^*Q_n^*] \rangle \overset{stat.}{=} \langle |Q_n|^2 \rangle = M. \tag{5.21}$$

Case: $\langle 4 \rangle = 0$

Again from Eq. (5.4) the 4-particle correlation, in Eq. (A.3), leads via recursive procedure to:

$$\langle 4 \rangle = 0 = \frac{|Q_n|^4 + |Q_{2n}|^2 - 2 \cdot \Re[Q_{2n} Q_n^* Q_n^*]}{M(M-1)(M-2)(M-3)} - 2\frac{2(M-2)|Q_n|^2 - M(M-3)}{M(M-1)(M-2)(M-3)}$$

$$\Leftrightarrow$$

$$|Q_n|^4 + \underbrace{|Q_{2n}|^2}_{rec.\ Eq.(5.11)} - 2 \cdot \underbrace{\Re[Q_{2n} Q_n^* Q_n^*]}_{rec.\ Eq.(5.21)} - 4(M-2) \cdot \underbrace{|Q_n|^2}_{rec.\ Eq.(5.11)} + 2M(M-3) = 0$$

$$\Rightarrow$$

$$|Q_n|^4 \overset{stat.}{=} M(2M-1). \tag{5.22}$$

Comparing the result obtained in Eq. (5.22) with Eq. (5.11), again something non trivial is happening.

When explicitly writing out the sum, we realize that somehow

$$|Q_n|^4 = Q_n Q_n Q_n^* Q_n^* = \sum_{i,j,k,l=1}^{M} e^{in(\varphi_i + \varphi_j - \varphi_k - \varphi_l)} \tag{5.23}$$

$$= M(2M-1) + \underbrace{\mathcal{O}(e^{i\Delta\bar{\varphi}})}_{\langle e^{i\Delta\bar{\varphi}} \rangle = 0}, \tag{5.24}$$

must be the case. Later we will see why. To conclude let's write:

$$|Q_n|^4 \overset{stat.}{=} \langle |Q_n|^4 \rangle = M(2M-1). \tag{5.25}$$

As the number of arguments in the m-particle correlation grow with the Bell numbers 1, 2, 5, 15, 52, 203, 877, 4140, 21147,... (sequence A000110 in the OEIS) [32], this used recursive process gets very inefficient. It's even worse if generally removing autocorrelations as in [37], $n!$ steps are necessary.

If one calculated the case $\langle 5 \rangle = ... = \langle k \rangle = 0$ or higher, one would have to solve all previous cases to get $\langle |Q_n|^k \rangle$. Instead let's try to solve $\langle |Q_n|^k \rangle$ directly. As we will see, by this approach the number of terms in one power k of $\langle |Q_n|^k \rangle$ grows with (1,) 1, 2, 3, 5, 7, 11, 15, 22, 30, 42, 56, 77, ... (sequence A000041 in the OEIS).

5.3 General $\langle |Q_n|^k \rangle$ random walk scaling

To obtain the general $\langle |Q_n|^k \rangle$ scaling, one has to find a way to calculate the number of autocorrelations, depending on the multiplicity M, for a given

power k.[1]

Just to clarify: We are not interested how exactly the autocorrelations, caused by the Q-vectors, look like, but only how many autocorrelations there are that survive the random walk. When generally removing autocorrelations additional terms appear [32, 37], whereas in our case some of these autocorrelations average to zero, because some are attached to other $\langle k \rangle$-particle correlations and these by themself are zero in the case of the random walk.

5.3.1 Even powers of k

Let us first look at the general scaling for even powers. We will see that the method found can easily be generalized to all other cases. In fact, the even powers are actually the most elaborate ones.

Generally we can write:

$$|Q_n|^k = \underbrace{Q_n Q_n ... Q_n^* Q_n^*}_{k-times} = \underbrace{\sum_{i,j,...,l,m=1}^{M}}_{k-indices} e^{in(\varphi_i+\varphi_j+...-\varphi_l-\varphi_m)}. \tag{5.26}$$

It is now interesting how often the exponent cancels to zero:

$$\varphi_i + \varphi_j + ... - \varphi_l - \varphi_m = 0. \tag{5.27}$$

Here each index $i, j, ...$ is summed separately from 1 to M.

Let us look at the second power ($k = 2$) as an example:

$$\varphi_i - \varphi_j = 0. \tag{5.28}$$

One notices immediately that this is the case for $i = j$, M-times. It is the most obvious and simplest general solution to Eq. (5.27): *all indices have the same value*. With higher powers, more possibilities arise and more and more solutions emerge.

Let us use a simpler notation. As we are only interested in the indices just the azimuthal-angles are numbered: $\varphi_i \Rightarrow 1, \varphi_j \Rightarrow 2..., \varphi_n \Rightarrow k$. We will separate the indices at $k/2$ with "|" because of the sign change. Next we will circle the indices that are the same e.g.:
$k = 8$: $\boxed{1\ 2\ 3}\ \textcircled{4}\ |\ \boxed{5\ 6\ 7}\ \textcircled{8}$.
Here three indices are the same and one is different. Of course we could have also said that 2,3,4 with 5,6,7 have the same indices value. But at first we

[1] Actually any combination of Q-vectors in the random walk. But these are actually less elaborate cases as we will see.

are merely interested in how many indices have to be the same, and not how many combinations there are to pick which are the same.

The first thing to notice in the case of all Q-vectors in the same harmonic n is, that we only have to evaluate half of the indices because of the change of the sign in the exponent.[1] The other half also has to have the same number of same indices, or the entire sum in Eq. (5.27) would not be 0. Therefore we only look at the first half ($k/2$-indices), and write "|" to remind us that there is always a corresponding set with an opposite sign. As example here are all possibilities for $k = 10$ and $k = 12$.

- $k = 10$:
  $\boxed{1\,2\,3\,4\,5}\,|$
  $\boxed{1\,2\,3\,4}\,\textcircled{5}\,|$
  $\boxed{1\,2\,3}\,\textcircled{4}\,\textcircled{5}\,| + \boxed{1\,2\,3}\,\boxed{4\,5}\,|^2$
  $\boxed{1\,2}\,\textcircled{3}\,\textcircled{4}\,\textcircled{5}\,| + \boxed{1\,2}\,\boxed{3\,4}\,\textcircled{5}\,|$ [3]
  $\textcircled{1}\,\textcircled{2}\,\textcircled{3}\,\textcircled{4}\,\textcircled{5}\,|$

- $k = 12$:
  $\boxed{1\,2\,3\,4\,5\,6}\,|$
  $\boxed{1\,2\,3\,4\,5}\,\textcircled{6}\,|$
  $\boxed{1\,2\,3\,4}\,\textcircled{5}\,\textcircled{6}\,| + \boxed{1\,2\,3\,4}\,\boxed{5\,6}\,|$
  $\boxed{1\,2\,3}\,\textcircled{4}\,\textcircled{5}\,\textcircled{6}\,| + \boxed{1\,2\,3}\,\boxed{4\,5\,6}\,| + \boxed{1\,2\,3}\,\boxed{4\,5}\,\textcircled{6}\,|$
  $\boxed{1\,2}\,\textcircled{3}\,\textcircled{4}\,\textcircled{5}\,\textcircled{6}\,| + \boxed{1\,2}\,\boxed{3\,4}\,\textcircled{5}\,\textcircled{6}\,| + \boxed{1\,2}\,\boxed{3\,4}\,\boxed{5\,6}\,|$
  $\textcircled{1}\,\textcircled{2}\,\textcircled{3}\,\textcircled{4}\,\textcircled{5}\,\textcircled{6}\,|$

As noted one has to be careful: *In one grouping (i are the same) the same or* ***only lower orders of groupings*** *(i are the same or i-n are the same) can appear additionally.*

This points out what we are actually doing. We are looking at all possible partitions and the rule that **only lower orders of groupings** are allowed, is analogue for Young-diagrams.

[1] This originates from the complex conjugate for the absolute value of a complex number.

[2] Note one does not distinguish between "1,2,4" same or "1,2,5" same. This is due to the fact that we will deal with these combinatorial choices later.

[3] "Two same" and "three same" was already dealt with previously, so there are no additional possibilities.

Partitions

When searching for the possible partitions it is completely analogue to the question of how many integer partitions there are for a number $n \in \mathbb{N}$. Using the partition function $P(n)$, which gives the total number of ways of writing the number n, we can find out how many terms we have to add in order to calculate the number of autocorrelations.
Example:

$$P(5) = 7. \tag{5.29}$$

All possibile partitions are:

$$\begin{aligned} 5 &= \\ &= 5 \\ &= 4 + 1 \\ &= 3 + 2 \\ &= 3 + 1 + 1 \\ &= 2 + 2 + 1 \\ &= 2 + 1 + 1 + 1 \\ &= 1 + 1 + 1 + 1 + 1. \end{aligned}$$

It turns out that the number of possible partitions we have to evaluate increases with $P(n)$ and are: (1,) 1, 2, 3, 5, 7, 11, 15, 22, 30, 42, 56, 77, 101, ... (sequence A000041 in the OEIS) [38]. It grows as an exponential function of the square root of its argument.

The conclusion is that, if the power k is even, one has $P(k/2)$ terms to add. One can also express the possible partitions with the help of Young-diagrams. Here is an example:

k=10:

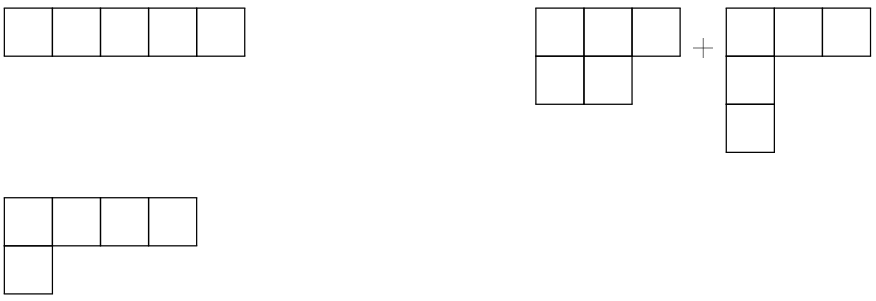

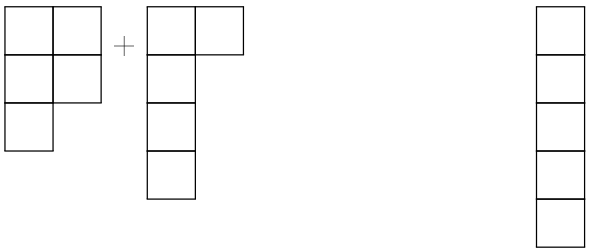

This is an analogue representation of the case of $k = 10$ which was shown above.[4] Unfortunately no closed-form expression for the partition function $P(n)$ is known and each Young-diagram has to be calculated in an recursive algorithm. This results in the fact that we cannot just directly write an analytic equation resolving this problem.

Permutations and combination of indices

In the following our only interest is how many permutations (arrangement of indices) and combinations (selection of indices from a collection of indices) are possible, but not yet how many variations (carrying out the indices from 1 to M) there are that result in the cancelling of the exponent of our Q-vector (in Eq. (5.27)).

We consider the **number of combinations to choose which indices are the same**. Here the order of selection doesn't matter, because they are all the same. Thus it is given by the binomial coefficient:

$$\binom{n}{k} = \binom{\text{number of indices places to choose}}{\text{number of same indices}}. \tag{5.30}$$

As an example let's look at $k = 10$, with $\boxed{1\ 2}\ \textcircled{3}\ \textcircled{4}\ \textcircled{5}\ | + \boxed{1\ 2}\ \boxed{3\ 4}\ \textcircled{5}\ |$:

$$\binom{\frac{k}{2} = 5}{2} + \binom{\frac{k}{2} = 5}{2}\binom{5 - 2 = 3}{2}. \tag{5.31}$$

In the second term we first choose to place the first *two coupled indices* and are then left with three places to pick in order to place the second *two coupled indices*.

After that we have a look at the number of **permutations (with repetition) of the indices**. This is of course not relevant for the case in which all indices are identical, as there is only one single option.[5]

[4] Horizontal boxes represent indices that are the same (circled in the other notation).

[5] Note: we are still not "filling in" values from 1 to M into the indices. Thus we have only one option. Later we can "fill in" and say that "all indices coupled" occurs M times.

For each indices there are $(\frac{k}{2})!$-possible permutations, but we can't distinguish between the indices that are the same and the *blocks* that have the equal number of *coupled indices*. Thus the **permutations with repetition** are:

$$\frac{(\frac{k}{2})!}{\prod\limits_{\text{all blocks}} (\text{number of same indices})! \prod\limits_{\text{frequency of blocks} \geq 2} (\text{number of same blocks})!}. \tag{5.32}$$

Example at $k = 10$, with $\boxed{1\ 2}\ \textcircled{3}\ \textcircled{4}\ \textcircled{5}\ | + \boxed{1\ 2}\ \boxed{3\ 4}\ \textcircled{5}\ |$:

$$\underbrace{\binom{5}{2}}_{from\ before} \cdot \frac{(\frac{k}{2}=5)!}{2!} + \underbrace{\binom{5}{2}\binom{3}{2}}_{from\ before} \cdot \frac{(\frac{k}{2}=5)!}{2!2!(\text{number of same blocks} = 2)!} \tag{5.33}$$

$$= \binom{5}{2}\frac{5!}{2!} + \binom{5}{2}\binom{3}{2}\frac{5!}{2!2!2!}. \tag{5.34}$$

Variations (without repetition) of indices

We finally have to *fill in* the possible values of the indices that run from 1 to M. This is a simple variation without repetition.

The first thing we have already realized was that the case of *all indices values are the same* occurs M-times. The other simple circumstance is when *all indices values are different*. For the first indices we have M options, for the second $M-1$, the third $M-2$,... That means we have the obvious case:

$$\underbrace{(\frac{k}{2})!}_{from\ before} \quad \frac{M!}{(M-\frac{k}{2})!}. \tag{5.35}$$

In all the other cases we can write symbolically:

$$\underbrace{*}_{stuff\ from\ before} \cdot \underbrace{M \cdot ... \cdot (M-n)}_{different\ things\ to\ fill}. \tag{5.36}$$

This results for $k = 10$, with $\boxed{1\ 2}\ (3)\ (4)\ (5)\ | + \boxed{1\ 2}\ \boxed{3\ 4}\ (5)\ |$ in:

$$\underbrace{\binom{5}{2}\frac{5!}{2!}}_{from\ before} \cdot \underbrace{M}_{\boxed{1\ 2}} \underbrace{(M-1)}_{3} \underbrace{(M-2)}_{4} \underbrace{(M-3)}_{5} \tag{5.37}$$

$$+ \underbrace{\binom{5}{2}\binom{3}{2}\frac{5!}{2!2!2!}}_{from\ before} \cdot \underbrace{M}_{\boxed{1\ 2}} \underbrace{(M-1)}_{\boxed{3\ 4}} \underbrace{(M-2)}_{5} \tag{5.38}$$

$$= \binom{5}{2}\frac{5!}{2!}\frac{M!}{(M-4)!} + \binom{5}{2}\binom{3}{2}\frac{5!}{2!2!2!}\frac{M!}{(M-3)!}. \tag{5.39}$$

5.3.2 General expression

In conclusion one could write symbolically:

$$\sum_{possible\ partitions} \text{(permutations w. rep.)} \cdot \text{(combinations no rep.)} \cdot \text{(variations no rep.)}.$$

The problem to write an analytic expression lies within the possible partitions and that no closed form for them is known.

Although no closed formula for all possible partitions is known, we can still think of a recursive algorithm and thus write a code that gives us the number of autocorrelations for any even power k of a Q-vector. A general recursive formula, written in C/C++ is given in the Appendix B.3.1 and a visual representation in Appendix B.3.2.

General isotropic conditions

One can generalise and look at cases in which ($n_i \in \mathbb{Z}$):

$$\sum_{i=1}^{M} n_i \varphi_i = 0. \tag{5.40}$$

These cases can be calculated analogous by using a *coupling* for the n_i-times reoccurring azimuthal angle φ_i, which cannot be broken down, and looking at the $|n_1| + |n_2| + ... + |n_{m-1}| + |n_m| = k$ power of the resulting

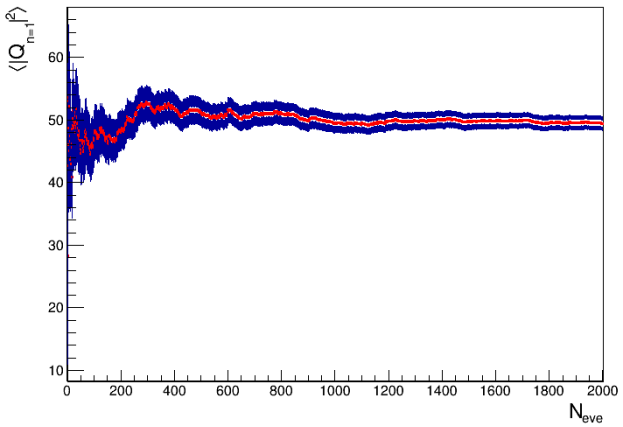

Figure 5.3: Here $M = 50$ random azimuthal angles were sampled from a uniform distribution and up to 2000-times simulated. In each simulation step the average $\langle |Q_{n=1}|^2 \rangle$ and the error was calculated. This resulted after the 2000 simulation steps in $\langle |Q_{n=1}|^2 \rangle = 49.4 \pm 1.1$, which is close to the expected value of 50 from Eq. (5.4) although the number of simulations was low. The blue band is the error and the red line the obtained result in each simulation step.

Q-vector ($m \in \mathbb{N}$):

$$|Q|^k = \underbrace{Q_{n_1} Q_{n_2} ... Q^*_{n_{m-1}} Q^*_{n_m}}_{m-times} = \underbrace{\sum_{i,j,...,l,m=1}^{M}}_{m-indices} e^{i(n_1\varphi_i + n_2\varphi_j + ... - n_{m-1}\varphi_l - n_m\varphi_m)}. \tag{5.41}$$

These *couplings* simplify the number of arguments that survive the random walk, meaning that the case $n_1 = n_2 = ... = n_{m-1} = n_m$ in Eq. (5.27) is actually the most elaborate one. Cases with these *couplings*, due to an uneven power, are calculated in the Appendix C.

5.3.3 Verification via simple Monte Carlo study

To verify Eq. (5.11), a very simple Monte Carlo study was done. To see how the random walk converges, the example $\langle |Q_{n=1}|^2 \rangle$ with $M = 50$ can be seen in Fig. 5.3.

In Fig. 5.4 results for different Multiplicities M of the random walk of $\langle |Q_n|^2 \rangle$, $\langle |Q_n|^4 \rangle$ and $\langle |Q_n|^6 \rangle$ are displayed. The lines are the expected results of the number of autocorrelations from Eqs. (5.11), (5.25) and (B.16). As

shown, the data points follow the expected result of $\mathcal{O}(e^{i\Delta\bar{\varphi}}) = 0$ quite well. Although in $\langle|Q_n|^6\rangle$ small effects of the central limit theorem, which result in $\mathcal{O}(e^{i\Delta\bar{\varphi}}) \neq 0$, can be seen. For example the data point $M = 18$ was simulated to be

$$\langle|Q_n|^6\rangle = (32247 \pm 37). \tag{5.42}$$

But from Eq. (B.16) one would expect $\langle|Q_n|^6\rangle = 32148$. Although this is only a 0.3% deviation from the originally expected value, the data point can't fit within error. This deviation could be explained by a *central limit effect* mentioned beforehand. It's effect is calculated in Appendix B.1.2.

5.3.4 Conclusion

As $\langle\mathcal{O}(e^{i\Delta\bar{\varphi}})\rangle$ has no main contributions in the random walk, only the parts where the azimuthal angles cancel to $(e^{i\cdot 0})$ remain dominant. This is of course precisely a part of the autocorrelation which is removed in the m-particle correlation in Eq. (4.5). Thus one could also write simply:

$$\langle|Q_n|^k\rangle = \underbrace{\sum_{i,j,\ldots,k,l=1}^{M} e^{in(\varphi_i+\varphi_j+\ldots-\varphi_k-\varphi_l)} - \sum_{\substack{i,j,\ldots,k,l=1 \\ (i\neq j\neq\ldots\neq k\neq l)}}^{M} e^{in(\varphi_i+\varphi_j+\ldots-\varphi_k-\varphi_l)}}_{autocorrelations \;+\; \langle\mathcal{O}(e^{i\Delta\bar{\varphi}})\rangle} \tag{5.43}$$

$$\langle|Q_n|^k\rangle \overset{stat.}{=} |Q_n|^k - \langle m\rangle\binom{M}{m}m! + \langle\mathcal{O}(e^{i\Delta\bar{\varphi}})\rangle \tag{5.44}$$

Since one still has to find out at all possible autocorrelation cases dependent on M this of course is more symbolically.

By setting a m-particle correlation to $\langle 2\rangle = \langle 3\rangle = \langle 4\rangle = 0$, one is able to solve, by *recursive procedure*, for Q-vectors in the appearing powers. Since the m-particle correlation already has all autocorrelations removed through Q-vectors, these solved for Q-vector powers now result in the autocorrelations they removed and thus giving the number of autocorrelations of $\langle|Q_n|^k\rangle$. One starts with $\langle|Q_n|^2\rangle$ from $\langle 2\rangle = 0$, which is the seed for the rest. But as mentioned before, just to get the $\langle|Q_n|^k\rangle$ autocorrelations, that pop out on the way, this recursive method would be very inefficient compared to directly evaluating $\langle|Q_n|^k\rangle$ in the manner just examined.

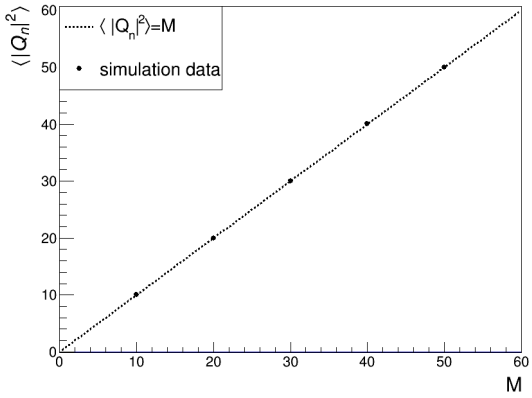

(a)

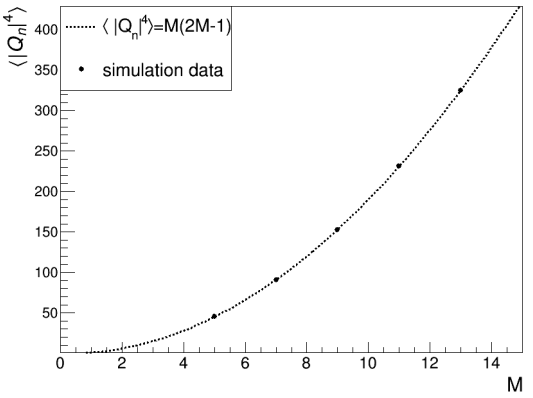

(b)

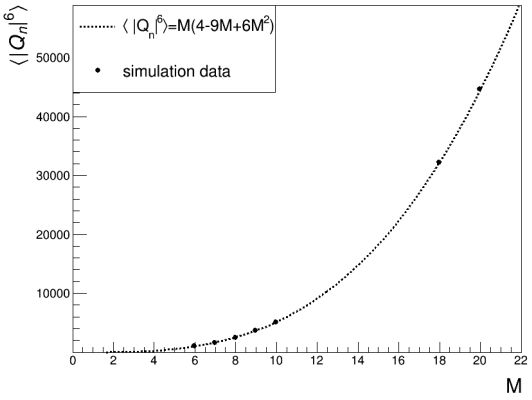

(c)

Figure 5.4: $\langle|Q_n|^2\rangle$, $\langle|Q_n|^4\rangle$ and $\langle|Q_n|^6\rangle$ calculated with 10.000.000 simulations per data point. The line is the expected value in the case of $\langle\mathcal{O}(e^{i\Delta\bar{\varphi}})\rangle = 0$.

5.4 Introduction of nonflow to the Random walk

5.4.1 Overcounting

After having understood the built-in Q-vector scaling in the random walk, we can use this knowledge to calculate an analytically exact nonflow scaling for track splitting. To do this we start with our 2-, 4-, 6- and 8-particle correlator and calculate the number of autocorrelations of the occurring Q-vectors. This is explicitly done in Appendix A.1. We will also need them for higher order Q-cumulants. Since we know now the autocorrelations of $|Q_n|^k$ as a function of M, we do not have to first recursively solve $\langle 5\rangle = \langle 6\rangle = \langle 7\rangle = \langle 8\rangle = ... = 0$ to get these additional Q-vector combinations which we would insert recursively.

We introduce nonflow by letting each track split k-times [13]. This corresponds to a realistic scenario in which due to detector inefficiencies each track gets split k times during reconstruction. But since we don't actually know how often a particle is split in the detector when observing, we must look at the total multiplicity M_{tot}. So if we start with a sample M per event and we take each particle k-times it results in:

$$M_{tot} = k \cdot M, \tag{5.45}$$

$$Q_{n,tot} = k \cdot Q_n. \tag{5.46}$$

In Appendix A.2 we implement Eq. (5.45) and Eq. (5.46) into our multiparticle correlators.

After that we can do a simple Monte Carlo study. We sample M azimuthal angles φ from a uniform distribution $[0, 2\pi)$, overcount them k-times and calculate the multiparticle correlation of our M_{tot} particles. Since only nonflow is present, we can compare our analytic expression for the nonflow scaling with the simulated nonflow correlation. These results for $k = 2, 3$ and 4 for the 4- and 6- particle correlator can be seen in Fig. 5.5. As shown, the results fit our analytical scaling nicely. The entire analytic expression of the 2-, 4-, 6- and 8- particle correlator can be found in the Appendix A.2.

5.4.2 Q-Cumulants

Now we insert our results from our previous section of the nonflow scaling of the multiparticle correlators into our Q-Cumulants from Eq. (4.2.1). Again we obtain an exact analytic expression how nonflow should scale. The next step is to check the results obtained in an analogue Monte Carlo study. The results can be seen in Fig. 5.6 and Fig. 5.7. As can be seen, the simulated data points fit perfectly to their expected nonflow behaviour.

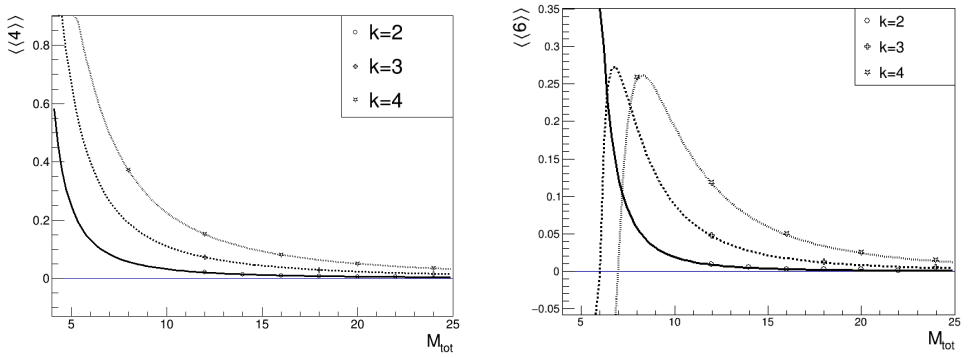

(a) (b)

Figure 5.5: The nonflow scaling of the 4- and 6-particle correlator compared to the analytically derived result of the nonflow scaling. The nonflow was induced by overcounting each particle k-times.

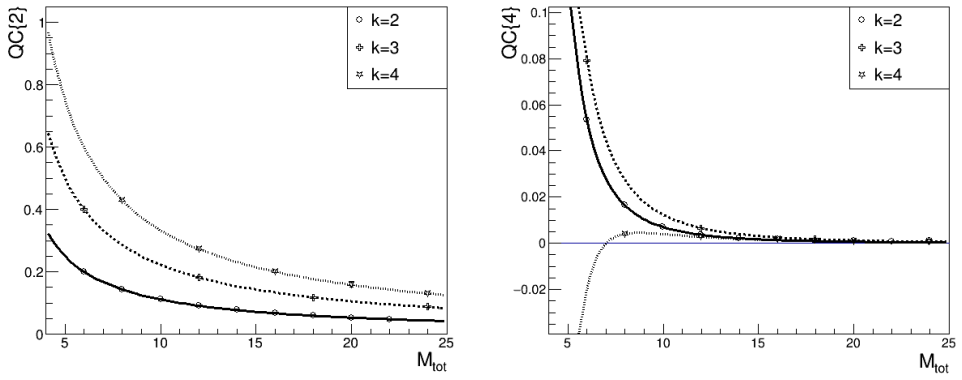

(a) (b)

Figure 5.6: Comparison of calculated nonflow correlation to expected nonflow scaling of $QC\{2\}$ and $QC\{4\}$ for $k = 2, 3$ and 4.

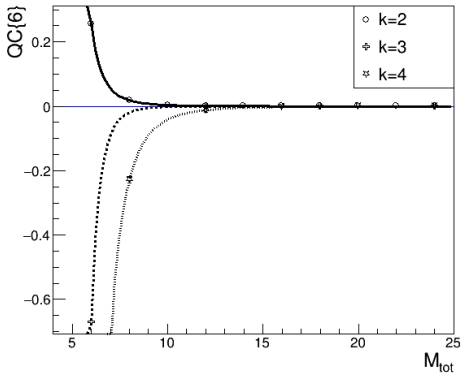

(a)

Figure 5.7: Comparison of calculated nonflow correlation to expected nonflow scaling of $QC\{6\}$ for $k = 2, 3$ and 4.

Further we can compare the nonflow sensitivity of the Q-cumulants to the m-multiparticle correlators for $k = 2, 3$ and 4. $QC\{4\}$, $QC\{6\}$ with their corresponding 4- and 6-particle correlator are shown in Fig. 5.8 with red indicating the Q-Cumulant.

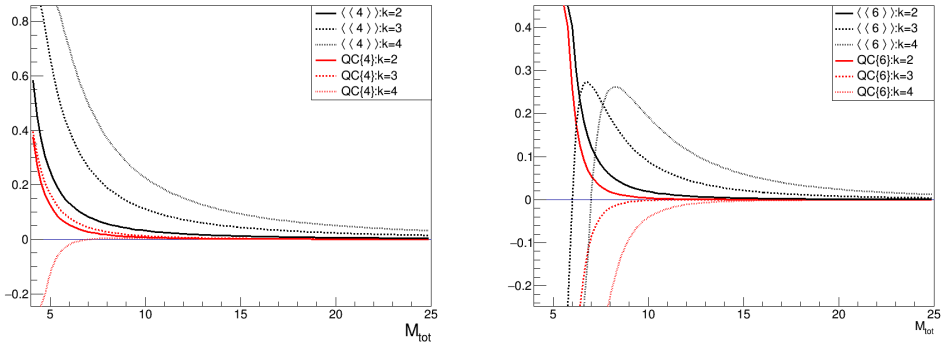

(a) (b)

Figure 5.8: Nonflow scaling of $QC\{4\}$, $QC\{6\}$ (in red) with their corresponding 4- ad 6-particle correlator for $k = 2, 3$ and 4.

We see that nonflow is suppressed faster in the Q-Cumulants than in the starting azimuthal correlators, as multiplicity increases. From Fig. 5.9a we see that $QC\{4\}$ only has 1% of the nonflow of the 4-particle correlator as soon as the multiplicity is larger than $M_{k=2} \geq 40$, $M_{k=3} \geq 100$ and $M_{k=4} \geq 200$. The same is the case in Fig. 5.9b in which we see that $QC\{6\}$ only has 1%

of the nonflow of the 6-particle correlator as soon as the multiplicity is larger then $M_{k=2} \geq 40$, $M_{k=3} \geq 70$ and $M_{k=4} \geq 130$. Further in Fig. 5.10 we

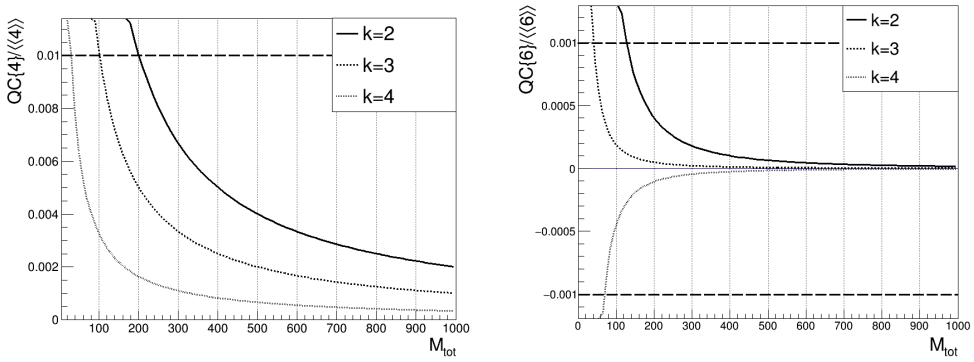

(a) (b)

Figure 5.9: The ratio of Q-Cumulant to corresponding multiparticle correlator. The line indicates when the Q-Cumulant is only 1% as sensitive as the corresponding multiparticle correlator.

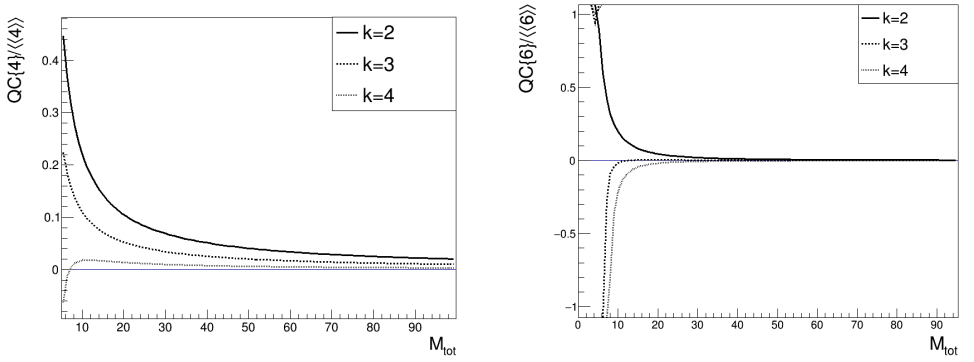

(a) (b)

Figure 5.10: The ratio of Q-cumulant to corresponding multiparticle correlator for low multiplicities M.

can see that also for low multiplicities $QC\{4\}$ is less sensitive than $\langle\langle 4\rangle\rangle$ to nonflow. The same is true for $QC\{6\}$ in comparison to $\langle\langle 6\rangle\rangle$, of course here the multiplicity M must be larger then 6.

5.4.3 Comparison of the probabilistic argument to exact nonflow scaling

The exact nonflow scaling expressions can be found in Appendix A.3.

The leading order terms for the considered multiparticle correlators in the limit of M_{tot} are:

$$\langle 2 \rangle \propto \frac{k-1}{M_{tot}} \tag{5.47}$$

$$\langle 4 \rangle \propto \frac{(k-1)(2k-2)}{M_{tot}^2} \tag{5.48}$$

$$\langle 6 \rangle \propto \frac{(k-1)\left(6k^2-12k+6\right)}{M_{tot}^3} \tag{5.49}$$

$$\langle 8 \rangle \propto \frac{24k^4-96k^3+144k^2-96k+24}{M_{tot}^4}. \tag{5.50}$$

This suggests a scaling of $\propto 1/M^{m/2}$. Therefore, in the limit of high Multiplicities the *probabilistic argument*, suggesting a scaling of $\approx 1/M^{m-1}$, underestimates the nonflow effects. If we compare our obtained nonflow scaling expressions to the *probabilistic argument* it turns out that it fails for specific k. This can be seen in Fig. 5.11 were the obtained nonflow scaling of the 4- and 6-particle correlator is compared to a fit of the *probabilistic argument* of: $a/M^{m-1}+b$ (a and b beeing fitting parameters). In the case of the 4-particle correlator in Fig. 5.11a we can see the probabilistic argument always underestimates the nonflow effect for $k = 2, 3$ and 4. On the other hand for the 6-particle correlator in Fig. 5.11b we can see that the probabilistic argument scaling fails at $k \geq 3$. The exact nonflow scaling expressions can be found in Appendix A.3. The leading orders of the Q-cumulants in the limit of M_{tot} are:

$$QC\{2\} \propto \frac{k-1}{M_{tot}}, \tag{5.51}$$

$$QC\{4\} \propto \frac{(k-1)\left(-k^2+5k-2\right)}{M_{tot}^3}, \tag{5.52}$$

$$QC\{6\} \propto \frac{4(k-1)\left(k^4-14k^3+44k^2-31k+6\right)}{M_{tot}^5}. \tag{5.53}$$

These follow the *probabilistic argument* perfectly.

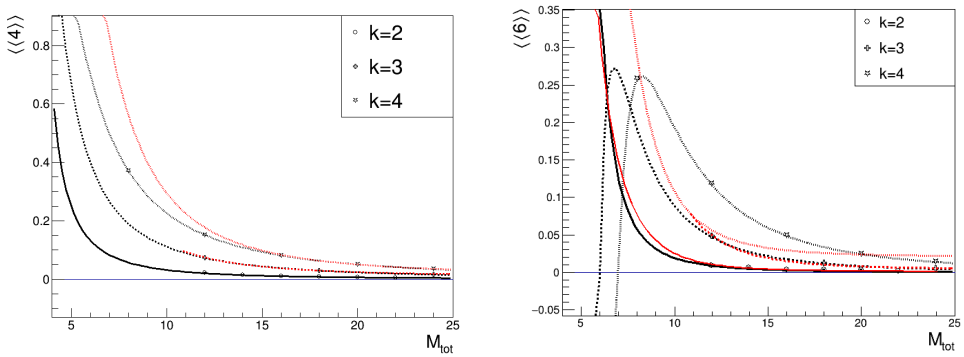

(a) (b)

Figure 5.11: Comparison of actual nonflow scaling with the *probabilistic argument*. Therefore $a/M^{m-1} + b$ was fitted to the data points, indicated in red.

Chapter 6

Summary

To summaries, first any flow or nonflow correlations were removed via random walk. Then the general scaling of Q-vectors in the random walk for any power or combination, in dependence of the multiplicity M, was derived and verified in a Monte Carlo study. After that nonflow was introduced by overcounting azimuthal angles, corresponding to track splitting. The results obtained of the Q-vectors in the random walk were then applied for a few chosen multiparticle correlators, and an analytic expression for the resulting nonflow found. This nonflow was then simulated in a Monte Carlo study. It's scaling was compared to the widely used probabilistic argument for high and low multiplicities. Analogue the nonflow scaling of the corresponding Q-Cumulants was derived and verified. At last the nonflow sensitivity of the direct multiparticle correlators was compared to the Q-Cumulants.

The next step is to confirm this nonflow scaling in Hijing, a heavy-ion collision simulator that models nonflow realistic, and having a closer look at p-p and p-A collisions and the appearing nonflow scaling.

Appendix A

Multiparticle correlations and Q-Cumulants

A.1 Multiparticle correlators

If we remove any autocorrelations via Q-vectors, this results in the following 2-/3-/4-/6- and 8-particle correlators [13]:

$$\begin{aligned}\langle 2\rangle &= \underbrace{\langle \exp[in(\varphi_1-\varphi_2)]\rangle}_{\varphi_1\neq\varphi_2} \\ &= \frac{|Q_n|^2 - M}{M(M-1)},\end{aligned} \tag{A.1}$$

$$\begin{aligned}\langle 3\rangle &= \underbrace{\langle \exp[in(2\varphi_1-\varphi_2-\varphi_3)]\rangle}_{\varphi_1\neq\varphi_2\neq\varphi_3} \\ &= \frac{\Re[Q_{2n}Q_n^*Q_n^*] - 2\cdot|Q_n|^2 - |Q_{2n}|^2 + 2M}{M(M-1)(M-2)},\end{aligned} \tag{A.2}$$

$$\begin{aligned}\langle 4\rangle &= \underbrace{\langle \exp[in(\varphi_1+\varphi_2-\varphi_3-\varphi_4)]\rangle}_{\varphi_1\neq\varphi_2\neq\varphi_3\neq\varphi_4} \\ &= \frac{|Q_n|^4 + |Q_{2n}|^2 - 2\cdot\Re[Q_{2n}Q_n^*Q_n^*]}{M(M-1)(M-2)(M-3)} - 2\frac{2(M-2)|Q_n|^2 - M(M-3)}{M(M-1)(M-2)(M-3)},\end{aligned} \tag{A.3}$$

$$\begin{aligned}\langle 6\rangle &= \underbrace{\langle \exp[in(\varphi_1+\varphi_2+\varphi_3-\varphi_4-\varphi_5-\varphi_6)]\rangle}_{\varphi_1\neq\varphi_2\neq\varphi_3\neq\varphi_4\neq\varphi_5\neq\varphi_6} \\ &= \frac{1}{\binom{M}{6}6!}\times[|Q_n|^6+9\cdot|Q_{2n}|^2|Q_n|^2-6\cdot\Re[Q_{2n}Q_nQ_n^*Q_n^*Q_n^*] \\ &\quad +4\cdot\Re[Q_{3n}Q_n^*Q_n^*Q_n^*]-12\cdot\Re[Q_{3n}Q_{2n}^*Q_n^*] \\ &\quad +18(kM-4)\Re[Q_{2n}Q_n^*Q_n^*]+4\cdot|Q_{3n}|^2 \\ &\quad -9(M-4)(|Q_n|^4+|Q_{2n}|^2)+18(M-2)(M-5)|Q_n|^2 \\ &\quad -6kM(kM-4)(kM-5)] \\ &\quad .\end{aligned} \tag{A.4}$$

$$\begin{aligned}\langle 8\rangle &\equiv \underbrace{\langle \exp[in(\varphi_1+\varphi_2+\varphi_3+\varphi_4-\varphi_5-\varphi_6-\varphi_7-\varphi_8)]\rangle}_{\varphi_1\neq\varphi_2\neq\varphi_3\neq\varphi_4\neq\varphi_5\neq\varphi_6\neq\varphi_7\neq\varphi_8} \\ &= \frac{1}{\binom{M}{8}8!}\times[|Q_n|^8-12\cdot Q_{2n}Q_nQ_nQ_n^*Q_n^*Q_n^*Q_n^* \\ &\quad +6\cdot Q_{2n}Q_{2n}Q_n^*Q_n^*Q_n^*Q_n^*+16\cdot Q_{3n}Q_nQ_n^*Q_n^*Q_n^*Q_n^* \\ &\quad -96\cdot Q_{3n}Q_nQ_{2n}^*Q_n^*Q_n^*-12\cdot Q_{4n}Q_n^*Q_n^*Q_n^*Q_n^* \\ &\quad -36\cdot Q_{2n}Q_{2n}Q_{2n}^*Q_n^*Q_n^*+96(M-6)\cdot Q_{2n}Q_nQ_n^*Q_n^*Q_n^* \\ &\quad +72\cdot Q_{4n}Q_{2n}^*Q_n^*+48\cdot Q_{3n}Q_nQ_{2n}^*Q_{2n}^* \\ &\quad -64(M-6)\cdot Q_{3n}Q_n^*Q_n^*Q_n^*+192(M-6)\cdot Q_{3n}Q_{2n}^*Q_n^* \\ &\quad -96\cdot Q_{4n}Q_{3n}^*Q_n^*-36\cdot Q_{4n}Q_{2n}^*Q_{2n}^* \\ &\quad -144(M-7)(M-4)Q_{2n}Q_n^*Q_n^*+36|Q_{4n}|^2+64|Q_{3n}|^2|Q_n|^2 \\ &\quad -64(M-6)|Q_{3n}|^2+9|Q_{2n}|^4+36|Q_n|^4|Q_{2n}|^2-144(M-6)k^4|Q_{2n}|^2|Q_n|^2 \\ &\quad +72(M-7)(M-4)(|Q_{2n}|^2+|Q_n|^4)-16(M-6)|Q_n|^6 \\ &\quad -96(M-7)(M-6)(M-2)|Q_{2n}|^2 \\ &\quad +24M(M-7)(M-6)(M-5)]\end{aligned} \tag{A.5}$$

A.2 Multiparticle correlators nonflow scaling

Induce nonflow to $\langle 2\rangle$

We start with the 2-particle correlation, Eq. (A.1), and apply Eq. (5.45) and Eq. (5.46). After that we insert our results of the random walk of the

Q-vectors ($|Q_n|^2$ from Eq. (5.11)):

$$\langle 2 \rangle \equiv \underbrace{\langle \exp[in(\varphi_1 - \varphi_2)] \rangle}_{\varphi_1 \neq \varphi_2} \tag{A.6}$$

$$= \frac{k^2|Q_n|^2 - kM}{kM(kM-1)} \tag{A.7}$$

$$= \frac{k-1}{kM-1} \tag{A.8}$$

$$= \frac{k-1}{M_{tot}-1}. \tag{A.9}$$

Induce nonflow to $\langle 4 \rangle$

Again we start with the 4-particle correlation, Eq. (A.3), and apply Eq. (5.45) and Eq. (5.46). Finally we replace our results of the random walk of the Q-vectors ($|Q_n|^2$ from Eq. (5.11), $\Re[Q_{2n}Q_n^*Q_n^*]$ from Eq. (5.21)):

$$\langle 4 \rangle \equiv \underbrace{\langle \exp[in(\varphi_1 + \varphi_2 - \varphi_3 - \varphi_4)] \rangle}_{\varphi_1 \neq \varphi_2 \neq \varphi_3 \neq \varphi_4} \tag{A.10}$$

$$= \frac{k^4|Q_n|^4 + k^2|Q_{2n}|^2 - 2 \cdot k^3 \Re[Q_{2n}Q_n^*Q_n^*]}{kM(kM-1)(kM-2)(kM-3)} \tag{A.11}$$

$$- 2\frac{2(kM-2)|Q_n|^2 - kM(kM-3)}{kM(kM-1)(kM-2)(kM-3)} \tag{A.12}$$

$$= -\frac{(k-1)\left(k^2 - 2kM_{tot} + 3k + 2M_{tot} - 6\right)}{(M_{tot}-3)(M_{tot}-2)(M_{tot}-1)}. \tag{A.13}$$

Induce nonflow to $\langle 6 \rangle$

To the 6-particle correlation, Eq. (A.4), we apply Eq. (5.45) and Eq. (5.46). After that we substitute our results of the random walk of the Q-vectors for all present combination and powers of them. They are explicitly calculated

in the Appendix B.1.

$$\langle 6\rangle \equiv \underbrace{\langle \exp[in(\varphi_1+\varphi_2+\varphi_3-\varphi_4-\varphi_5-\varphi_6)]\rangle}_{\varphi_1\neq\varphi_2\neq\varphi_3\neq\varphi_4\neq\varphi_5\neq\varphi_6} \tag{A.14}$$

$$= \frac{1}{\binom{kM}{6}6!}\times[k^6|Q_n|^6+9\cdot k^4|Q_{2n}|^2|Q_n|^2-6\cdot k^5\Re[Q_{2n}Q_nQ_n^*Q_n^*Q_n^*]] \tag{A.15}$$

$$+4\cdot k^4\Re[Q_{3n}Q_n^*Q_n^*Q_n^*]-12\cdot k^3\Re[Q_{3n}Q_{2n}^*Q_n^*] \tag{A.16}$$

$$+18(kM-4)k^3\Re[Q_{2n}Q_n^*Q_n^*]+4k^2\cdot|Q_{3n}|^2 \tag{A.17}$$

$$-9(kM-4)(k^4|Q_n|^4+k^2|Q_{2n}|^2)+18(kM-2)(kM-5)k^2|Q_n|^2 \tag{A.18}$$

$$-6kM(kM-4)(kM-5)] \tag{A.19}$$

$$=\frac{(-1+k)(120-2k(50+27M)+k^4(4-9M+6M^2)}{(-5+kM)(-4+kM)(-3+kM)(-2+kM)(-1+kM)} \tag{A.20}$$

$$-\frac{2k^3(-8+9M+6M^2)+k^2(-16+81M+6M^2))}{(-5+kM)(-4+kM)(-3+kM)(-2+kM)(-1+kM)} \tag{A.21}$$

$$=\frac{(k-1)(4k^4+k^3(16-9M_{tot})+2k^2\left(3M_{tot}^2-9M_{tot}-8\right))}{(M_{tot}-5)(M_{tot}-4)(M_{tot}-3)(M_{tot}-2)(M_{tot}-1)} \tag{A.22}$$

$$+\frac{(k-1)k\left(-12M_{tot}^2+81M_{tot}-100\right)+6\left(M_{tot}^2-9M_{tot}+20\right)}{(M_{tot}-5)(M_{tot}-4)(M_{tot}-3)(M_{tot}-2)(M_{tot}-1)}. \tag{A.23}$$

Induce nonflow to $\langle 8\rangle$

To the 8-particle correlation, Eq. (A.5), we apply Eq. (5.45) and Eq. (5.46). Then we substitute our results of the random walk of the Q-vectors for all present combination and powers of them. They are explicitly calculated in

the Appendix B.2.

$$\langle 8\rangle \equiv \underbrace{\langle \exp[in(\varphi_1+\varphi_2+\varphi_3+\varphi_4-\varphi_5-\varphi_6-\varphi_7-\varphi_8)]\rangle}_{\varphi_1\neq\varphi_2\neq\varphi_3\neq\varphi_4\neq\varphi_5\neq\varphi_6\neq\varphi_7\neq\varphi_8} \tag{A.24}$$

$$= \frac{1}{\binom{kM}{8}8!}\times[k^8|Q_n|^8 - 12\cdot k^7 Q_{2n}Q_nQ_nQ_n^*Q_n^*Q_n^* \tag{A.25}$$

$$+ 6\cdot k^6 Q_{2n}Q_{2n}Q_n^*Q_n^*Q_n^*Q_n^* + 16\cdot k^6 Q_{3n}Q_nQ_n^*Q_n^*Q_n^*Q_n^* \tag{A.26}$$

$$- 96\cdot k^5 Q_{3n}Q_nQ_{2n}^*Q_n^*Q_n^* - 12\cdot k^5 Q_{4n}Q_n^*Q_n^*Q_n^*Q_n^* \tag{A.27}$$

$$- 36\cdot k^5 Q_{2n}Q_{2n}Q_{2n}^*Q_n^*Q_n^* + 96(kM-6)\cdot k^5 Q_{2n}Q_nQ_n^*Q_n^*Q_n^* \tag{A.28}$$

$$+ 72\cdot k^4 Q_{4n}Q_{2n}^*Q_n^*Q_n^* + 48\cdot k^4 Q_{3n}Q_nQ_{2n}^*Q_{2n}^* \tag{A.29}$$

$$- 64(kM-6)\cdot k^4 Q_{3n}Q_n^*Q_n^*Q_n^* + 192(kM-6)\cdot k^3 Q_{3n}Q_{2n}^*Q_n^* \tag{A.30}$$

$$- 96\cdot k^3 Q_{4n}Q_{3n}^*Q_n^* - 36\cdot k^3 Q_{4n}Q_{2n}^*Q_{2n}^* \tag{A.31}$$

$$- 144(kM-7)(kM-4)k^3 Q_{2n}Q_n^*Q_n^* + 36k^2|Q_{4n}|^2 + 64k^4|Q_{3n}|^2|Q_n|^2 \tag{A.32}$$

$$- 64(kM-6)k^2|Q_{3n}|^2 + 9k^4|Q_{2n}|^4 + 36k^6|Q_n|^4|Q_{2n}|^2 \tag{A.33}$$

$$- 144(kM-6)k^4|Q_{2n}|^2|Q_n|^2 \tag{A.34}$$

$$+ 72(kM-7)(kM-4)(k^2|Q_{2n}|^2 + k^4|Q_n|^4) - 16(kM-6)k^6|Q_n|^6 \tag{A.35}$$

$$- 96(kM-7)(kM-6)(kM-2)k^2|Q_{2n}|^2 \tag{A.36}$$

$$+ 24kM(kM-7)(kM-6)(kM-5)] \tag{A.37}$$

$$= \frac{k^7\left(24M^3-72M^2+82M-33\right)-4k^6\left(24M^3-50M+33\right)}{(kM-7)(kM-6)(kM-5)(kM-4)(kM-3)(kM-2)(kM-1)} \tag{A.38}$$

$$+ \frac{2k^5\left(72M^3+432M^2-448M+153\right)}{(kM-7)(kM-6)(kM-5)(kM-4)(kM-3)(kM-2)(kM-1)} \tag{A.39}$$

$$- \frac{8k^4\left(12M^3+234M^2+158M-87\right)}{(kM-7)(kM-6)(kM-5)(kM-4)(kM-3)(kM-2)(kM-1)} \tag{A.40}$$

$$+ \frac{k^3\left(24M^3+1512M^2+6754M-1521\right)}{(kM-7)(kM-6)(kM-5)(kM-4)(kM-3)(kM-2)(kM-1)} \tag{A.41}$$

$$- \frac{4k^2\left(108M^2+1846M+1329\right)+12k(214M+875)-5040}{(kM-7)(kM-6)(kM-5)(kM-4)(kM-3)(kM-2)(kM-1)}. \tag{A.42}$$

Rewriting with the total multiplicity M_{tot} results in:

$$\langle 8 \rangle = \tag{A.43}$$

$$= \frac{-4k^2\left(\frac{108M_{tot}^2}{k^2}+\frac{1846M_{tot}}{k}+1329\right)}{(M_{tot}-7)(M_{tot}-6)(M_{tot}-5)(M_{tot}-4)(M_{tot}-3)(M_{tot}-2)(M_{tot}-1)} \tag{A.44}$$

$$- \frac{4k^6\left(\frac{24M_{tot}^3}{k^3}-\frac{50M_{tot}}{k}+33\right)}{(M_{tot}-7)(M_{tot}-6)(M_{tot}-5)(M_{tot}-4)(M_{tot}-3)(M_{tot}-2)(M_{tot}-1)} \tag{A.45}$$

$$+ \frac{k^3\left(\frac{24M_{tot}^3}{k^3}+\frac{1512M_{tot}^2}{k^2}+\frac{6754M_{tot}}{k}-1521\right)}{(M_{tot}-7)(M_{tot}-6)(M_{tot}-5)(M_{tot}-4)(M_{tot}-3)(M_{tot}-2)(M_{tot}-1)} \tag{A.46}$$

$$+ \frac{k^7\left(\frac{24M_{tot}^3}{k^3}-\frac{72M_{tot}^2}{k^2}+\frac{82M_{tot}}{k}-33\right)}{(M_{tot}-7)(M_{tot}-6)(M_{tot}-5)(M_{tot}-4)(M_{tot}-3)(M_{tot}-2)(M_{tot}-1)} \tag{A.47}$$

$$+ \frac{2k^5\left(\frac{72M_{tot}^3}{k^3}+\frac{432M_{tot}^2}{k^2}-\frac{448M_{tot}}{k}+153\right)}{(M_{tot}-7)(M_{tot}-6)(M_{tot}-5)(M_{tot}-4)(M_{tot}-3)(M_{tot}-2)(M_{tot}-1)} \tag{A.48}$$

$$- \frac{8k^4\left(\frac{12M_{tot}^3}{k^3}+\frac{234M_{tot}^2}{k^2}+\frac{158M_{tot}}{k}-87\right)}{(M_{tot}-7)(M_{tot}-6)(M_{tot}-5)(M_{tot}-4)(M_{tot}-3)(M_{tot}-2)(M_{tot}-1)} \tag{A.49}$$

$$+ \frac{12k\left(\frac{214M_{tot}}{k}+875\right)-5040}{(M_{tot}-7)(M_{tot}-6)(M_{tot}-5)(M_{tot}-4)(M_{tot}-3)(M_{tot}-2)(M_{tot}-1)}. \tag{A.50}$$

A.3 Q-Cumulants nonflow scaling

Now we introduce our results from Eq. (A.9), Eq. (A.13) and Eq. (A.23) into our Q-Cumulants:

$$QC\{2\} \equiv \langle\langle 2 \rangle\rangle = \frac{k-1}{kM-1} = \frac{k-1}{M_{tot}-1} \tag{A.51}$$

$$\begin{aligned} QC\{4\} &\equiv \langle\langle 4\rangle\rangle - 2\cdot\langle\langle 2\rangle\rangle^2 \\ &= -\frac{(k-1)[k^3M - k^2(5M+1) + k(2M+9) - 6]}{(kM-1)^2(kM-2)(kM-3)} \\ &= -\frac{(k-1)\left(k^2(M_{tot}-1) + k(9-5M_{tot}) + 2(M_{tot}-3)\right)}{(M_{tot}-3)(M_{tot}-2)(M_{tot}-1)^2} \end{aligned} \tag{A.52}$$

$$\begin{aligned} QC\{6\} &\equiv \langle\langle 6\rangle\rangle - 9\cdot\langle\langle 2\rangle\rangle\langle\langle 4\rangle\rangle + 12\cdot\langle\langle 2\rangle\rangle^3 \\ &= \frac{4(-1+k)(120 + k^6M^2 - 2k^5M(1+7M) - 2k(170+27M))}{(-5+kM)(-4+kM)(-3+kM)(-2+kM)(-1+kM)^3} \\ &+\frac{4(-1+k)(k^2(266+227M+6M^2) - k^3(41+238M+31M^2))}{(-5+kM)(-4+kM)(-3+kM)(-2+kM)(-1+kM)^3} \\ &+\frac{4(-1+k)(k^4(1+55M+44M^2))}{(-5+kM)(-4+kM)(-3+kM)(-2+kM)(-1+kM)^3} \\ &= \frac{4(k-1)\left(k^4(M_{tot}-1)^2 + k^3\left(-14M_{tot}^2 + 55x - 41\right)\right)}{(M_{tot}-5)(M_{tot}-4)(M_{tot}-3)(M_{tot}-2)(M_{tot}-1)^3} \\ &+\frac{4(k-1)\left(k^2\left(44M_{tot}^2 - 238M_{tot} + 266\right) + k\left(-31M_{tot}^2 + 227M_{tot} - 340\right)\right)}{(M_{tot}-5)(M_{tot}-4)(M_{tot}-3)(M_{tot}-2)(M_{tot}-1)^3} \\ &+\frac{4(k-1)\left(6\left(M_{tot}^2 - 9M_{tot} + 20\right)\right)}{(M_{tot}-5)(M_{tot}-4)(M_{tot}-3)(M_{tot}-2)(M_{tot}-1)^3}. \end{aligned} \tag{A.53}$$

In the last step we replaced $k \cdot M = M_{tot}$.

Appendix B

Random walk of $\langle |Q_n|^k \rangle$

B.1 $\langle \mathcal{O}(e^{i\Delta\bar{\varphi}}) \rangle$ contributions and central limit effects

Let's first have a look at the case if one did not consider the central limit theorem and then later calculate its effects. For further calculations we assume the *flow-principle* as fulfilled. So all azimuthal angles φ_i are independent of each other and follow the same underlying p.d.f., with the identical $\langle \varphi_i \rangle$ and $(\Delta\varphi_i)^2$.

Of course to generally calculate the expectation value of a function $f(\varphi_1, ..., \varphi_n)$ with the p.d.f. $p(\varphi_1, ..., \varphi_n)$ one has to evaluate:

$$\langle f(\varphi_1, ..., \varphi_n) \rangle = \int_{-\infty}^{+\infty} \cdots \int_{-\infty}^{+\infty} f(\varphi_1, ..., \varphi_n) p(\varphi_1, ..., \varphi_n) d\varphi_1 \cdots d\varphi_n. \quad \text{(B.1)}$$

Furthermore, we are looking at Q-vector powers in different harmonics:

$$f(\varphi_1, ..., \varphi_n) = e^{i(\pm m_1\varphi_1 \pm ... \pm m_n\varphi_n)}, \quad \text{(B.2)}$$

with $m_1, ..., m_n \in \mathbb{N}$ while the whole exponent follows the *isotropic condition*.

B.1.1 $\langle \mathcal{O}(e^{i\Delta\bar{\varphi}}) \rangle = 0$ is the case

Since we are looking at the random walk, each azimuthal angle φ_i is uniformly distributed $[0, 2\pi)$. Thus the normalized p.d.f. is:

$$p(\varphi_1, ..., \varphi_n) = \frac{1}{(2\pi)^n} \Theta(2\pi - \varphi_1)\Theta(\varphi_1) \cdots \Theta(2\pi - \varphi_n)\Theta(\varphi_n). \quad \text{(B.3)}$$

We can now calculate the expectation value:

$$\langle e^{i(\pm m_1\varphi_1 \pm ... \pm m_n\varphi_n)} \rangle = \frac{1}{(2\pi)^n} \int_0^{2\pi} \cdots \int_0^{2\pi} e^{i(\pm m_1\varphi_1 \pm ... \pm m_n\varphi_n)} d\varphi_1 \cdots d\varphi_n \tag{B.4}$$

$$= \frac{1}{(2\pi)^n} \int_0^{2\pi} \cdots \int_0^{2\pi} e^{i(\pm m_2\varphi_1 \pm ... \pm m_n\varphi_n)} d\varphi_2 \cdots d\varphi_n \underbrace{\int_0^{2\pi} e^{im_1\varphi_1} d\varphi_1}_{m_i \in \mathbb{N},\ \Rightarrow\ =0} \tag{B.5}$$

$$= 0. \tag{B.6}$$

B.1.2 $\langle \mathcal{O}(e^{i\Delta\bar{\varphi}}) \rangle \neq 0$ is the case

Central limit theorem: If $X_1, ..., X_N$ are independent random variables with identical p.d.f. ($\langle X_i \rangle$ and $(\Delta X_i)^2$), then the p.d.f of $Y = X_1 + ... + X_N$, in the limit of $N \to \infty$, is given by [39]:

$$p_\infty(Y) = \frac{1}{\sqrt{2\pi N(\Delta X)^2}} \cdot e^{-\frac{(Y - \langle X \rangle N)^2}{2(\Delta X)^2 N}}. \tag{B.7}$$

Since all boundary conditions are fulfilled, let us apply the now emerging normal distribution and calculate with the random variable $\bar{\varphi} = \pm m_1\varphi_1 \pm ... \pm m_n\varphi_n$. Notice here, that the condition $Y = X_1 + ... + X_N$ is still fulfilled as we can simply shift their identical p.d.f. to a uniform distribution between $[-\pi, \pi)$. This p.d.f. is now symmetric and a positive or negative value is equally probable. Thus it doesn't matter if we add or subtract any φ_i. Furthermore we are not adding N random variables but $\tilde{n} = \sum_{i=1}^n m_i$. The *central limit effect* $\Delta_{centr.lim.}$ results in[1]:

$$\Delta_{centr.lim.} = \langle e^{i\bar{\varphi}} \rangle = \frac{1}{\sqrt{2\pi\tilde{n}(\Delta\bar{\varphi})^2}} \cdot \int_{-\infty}^{+\infty} d\bar{\varphi} e^{i\bar{\varphi}} e^{-\frac{(\bar{\varphi} - \langle\varphi_i\rangle\tilde{n})^2}{2(\Delta\varphi_i)^2\tilde{n}}} \tag{B.8}$$

$$= e^{i\cdot\tilde{n}\langle\varphi_i\rangle - \frac{\tilde{n}(\Delta\varphi_i)^2}{2}} = e^{i\cdot\langle\varphi_i\rangle\sum_{i=1}^n m_i - \frac{(\Delta\varphi_i)^2\sum_{i=1}^n m_i}{2}}. \tag{B.9}$$

This is true if $\Re[2(\Delta\varphi_i)^2\tilde{n}] > 0$ which is of course the case since $\tilde{n}$ is the total sum of $m_i\varphi_i$ which we have, and thus $\tilde{n} \in \mathbb{N}$. We can calculate $(\Delta\varphi_i)^2$ by $(\Delta\varphi_i)^2 = \langle\varphi_i^2\rangle - \langle\varphi_i\rangle^2$.

For our random walk, uniformly distributed between $[-\pi, \pi)$, we obviously get:

$$\langle\varphi_i\rangle = \frac{1}{2\pi} \int_{-\pi}^{\pi} d\varphi_i\varphi_i = 0, \tag{B.10}$$

[1] This result was obtained by the usage of Mathematica [40].

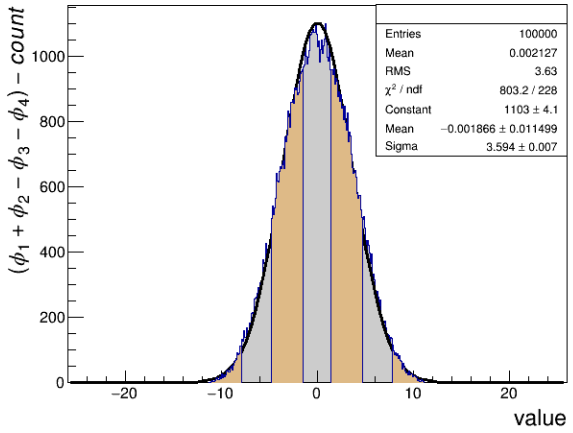

Figure B.1: The central limit effect of the combination of only four, each uniformly sampled, azimuthal angles φ_i and the resulting normal distribution after 100 000 iterations.

$$\Delta\varphi_i^2 = \langle\varphi_i^2\rangle - \langle\varphi_i\rangle^2 = \frac{1}{2\pi}\int_{-\pi}^{\pi} d\varphi_i \varphi_i^2 = \frac{\pi^2}{3}. \tag{B.11}$$

Substituting in Eq. (B.9) it results in:

$$\Delta_{centr.lim.} = \langle e^{i\bar{\varphi}}\rangle = e^{-\frac{\tilde{n}\pi^2}{6}} = e^{-\frac{\pi^2 \sum_{i=1}^{n} m_i}{6}}. \tag{B.12}$$

As illustrated in Fig. B.1 already four linear combined azimuthal angles $\bar{\varphi}' = \varphi_i + \varphi_j - \varphi_k - \varphi_l$ ($\tilde{n} = 4$), each of them sampled from a uniform distribution, result in a collective approximate normal distribution after only 100 000 repetitions. 100 000 terms with these $\bar{\varphi}'$ combinations in the fourth power of a Q-vector are already met at Multiplicity of M>19. The brown and grey strips have a width of π and indicate which parts of the distribution will result in a positive (grey) or negative (brown) contribution to the Q-vector scaling in $\Re e^{i\bar{\varphi}'} = \cos\bar{\varphi}'$.[2]

The $|Q_n|^6$ case with *central limit effects*:

Now looking at Eq. (B.12) we see that we get a deviation depending on $\tilde{n}$. Thus we have to find out how often $\tilde{n}$ occurs. The first thing to realise is, that $\tilde{n}$ is even, since the whole expression $\bar{\varphi} = \pm m_1\varphi_1 \pm ... \pm m_n\varphi_n$ still has

[2]Note: in the statistical limit $\langle e^{i\bar{\varphi}}\rangle = e^{i\langle\bar{\varphi}\rangle}$ is the case. This is due to the fact that in $\sum_{n=0}^{\infty}(i\bar{\varphi})^n/n!$, $\langle\bar{\varphi}^n\rangle = \langle\bar{\varphi}\rangle^n$ happens, since $\Delta\bar{\varphi}/N = 1/N(\langle\bar{\varphi}^2\rangle - \langle\bar{\varphi}\rangle^2) \to 0$, because of the behaviour of the central limit theorem in the statistical limit.

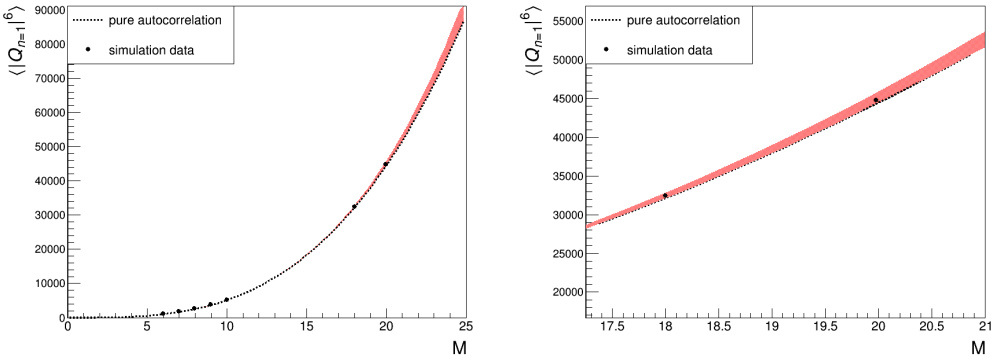

(a) (b)

Figure B.2: The Q-vector scaling of $|Q_n|^6$ with central limit effect highlighted in red.

to follow the *isotropic condition* (e.g. $\bar{\varphi} = 2\varphi_1 + \varphi_2 - 2\varphi_3 - \varphi_4$ in $e^{in(\bar{\varphi})}$). We can estimate the central limit effect by looking at the dominant case were all azimuthal angles φ_i are different (the majority of the terms with $\tilde{n} = 6$). This leads to

$$\Delta_{centr.lim.} \approx \frac{M!}{(M-6)!} e^{-\pi^2}. \tag{B.13}$$

In Fig. B.2a and as close up in Fig. B.2b, the deviation from the pure autocorrelations through the central limit effect is indicated by the red band. As can be seen, the simulated values now lay perfectly within. But as mentioned the central limit effects seen are very small and can be neglected.

B.2 Derivation of $\langle |Q_n|^k \rangle$: $k = 2$, $k = 4$, $k = 6$, $k = 8$, $k = 10$

All these autocorrelations have been separately verified with Mathematica [40] up to $k = 10$.

$\langle |Q_n|^2 \rangle$:

(1) $| \Rightarrow$ M
This sums up to:

$$\langle |Q_n|^2 \rangle = M + \langle \mathcal{O}(e^{i\Delta\bar{\varphi}}) \rangle. \tag{B.14}$$

$\langle|Q_n|^4\rangle$:

$\boxed{1\ 2}\ |\Rightarrow \mathrm{M}$
$(1)\ (2)\ |\Rightarrow 2!\frac{M!}{(M-2)!}$
This sums up to:

$$\langle|Q_n|^4\rangle = M(-1+2M) + \langle\mathcal{O}(e^{i\Delta\bar{\varphi}})\rangle. \tag{B.15}$$

$\langle|Q_n|^6\rangle$:

$\boxed{1\ 2\ 3}\ |\Rightarrow \mathrm{M}$
$\boxed{1\ 2}\ (3)\ |\Rightarrow \frac{1}{2!}3!\binom{3}{2}M(M-1)$
$(1)\ (2)\ (3)\ |\Rightarrow 3!\frac{M!}{(M-3)!}$
This sums up to:

$$\langle|Q_n|^6\rangle = M(4-9M+6M^2) + \langle\mathcal{O}(e^{i\Delta\bar{\varphi}})\rangle. \tag{B.16}$$

$\langle|Q_n|^8\rangle$:

$\boxed{1\ 2\ 3\ 4}\ |\Rightarrow \mathrm{M}$
$\boxed{1\ 2\ 3}\ (4)\ |\Rightarrow \frac{1}{3!}4!\binom{4}{3}M(M-1)$
$\boxed{1\ 2}\ (3)\ (4)\ |\ +\ \boxed{1\ 2}\ \boxed{3\ 4}\ |$
$\Rightarrow \frac{1}{2!}4!\binom{4}{2}M(M-1)(M-2)\ +\ \frac{1}{2!2!2!}4!\binom{4}{2}\binom{4-2}{2}M(M-1)$
$(1)\ (2)\ (3)\ (4)\ |\Rightarrow 4!\frac{M!}{(M-4)!}$
This sums up to:

$$\langle|Q_n|^8\rangle = M(-33+82M-72M^2+24M^3) + \langle\mathcal{O}(e^{i\Delta\bar{\varphi}})\rangle. \tag{B.17}$$

$\langle|Q_n|^{10}\rangle$:

$\boxed{1\ 2\ 3\ 4\ 5}\ |\Rightarrow \mathrm{M}$
$\boxed{1\ 2\ 3\ 4}\ (5)\ |\Rightarrow \frac{1}{4!}5!\binom{5}{4}M(M-1)$
$\boxed{1\ 2\ 3}\ (4)\ (5)\ |\ +\ \boxed{1\ 2\ 3}\ \boxed{4\ 5}\ |$
$\Rightarrow \frac{1}{3!}5!\binom{5}{3}M(M-1)(M-2)\ +\ \frac{1}{2!3!}5!\binom{5}{3}\binom{2}{2}M(M-1)$
$\boxed{1\ 2}\ (3)\ (4)\ (5)\ |\ +\ \boxed{1\ 2}\ \boxed{3\ 4}\ (5)\ |$
$\Rightarrow \frac{1}{2!}5!\binom{5}{2}M(M-1)(M-2)(M-3)\ +\ \frac{1}{2!2!2!}5!\binom{5}{2}\binom{3}{2}M(M-1)(M-2)$

① ② ③ ④ ⑤ | $\Rightarrow (\frac{k}{2})! \frac{M!}{(M-5)!}$
This sums up to:

$$\langle|Q_n|^{10}\rangle = M(456 - 1225M + 1250M^2 - 600M^3 + 120M^4) + \langle\mathcal{O}(e^{i\Delta\bar{\varphi}})\rangle. \tag{B.18}$$

B.3 Algorithm for any even power $\langle|Q_n|^k\rangle$

B.3.1 C/C++ Code for number of autocorrelations in any even power $\langle|Q_n|^k\rangle$

Constrains: k must be even, $M \geq k$.

```
#include <iostream>
#include <fstream>
#include <algorithm>
#include <vector>

using namespace std;

void printArray(int p[], int n)
{

    for (int i = 0; i < n; i++)
    {
        cout << p[i] << "␣";
    }

    cout << endl;
}

vector<int> storePartitions(int p[], int n)
{
    vector<int> rowPart;

    for (int i = 0; i < n; i++)
    {
        rowPart.push_back(p[i]);
    }

    return rowPart;
}

long int fakultaet(long int x)
{
        if(x > 1) {
```

```
                return x * fakultaet(x-1);
        }else {
                return 1;
        }
}

//calculate all combinations with no repetitions
long int combinations(int k, vector<int> *rowPart)
{
    long int combinations = 1;
    long int leftOptions = 0;
    long int temp = 0;

    for(int i=0; i<rowPart->size(); i++)
    {
        if(!(rowPart->at(i)==1))
        {
            leftOptions = k/2-temp;
            combinations *= fakultaet(leftOptions)/
            (fakultaet(rowPart->at(i))*fakultaet(leftOptions-rowPart->at(i)));
            temp = rowPart->at(i);
        }
    }

    return(combinations);
}

//calculate all permutations with repetition
long int permutations(int k, vector<int> *rowPart, vector<int> *sameElementsPart)
{
    long int counterPermutatations = fakultaet(k/2);

    long int partElementsPart = 1;
    long int partSameElementsPart = 1;

    for(int i=0; i<rowPart->size(); i++)
    {
        partElementsPart *= fakultaet(rowPart->at(i));
    }
    for(int i=0; i<sameElementsPart->size(); i++)
    {
        partSameElementsPart *= fakultaet(sameElementsPart->at(i));
    }

    return(counterPermutatations/(partElementsPart*partSameElementsPart));

}

//calculate all variations with no repetitions
```

```
long int variations(int numberPartElements, int M)
{
        if(numberPartElements > 0)
        {
                return M * variations(numberPartElements-1, M-1);
        }
        else
        {
                return 1;
        }
}

//find how many identical partitions (excluding 1) exist
vector<int> numberSameEntries(vector<int> rowPart)
{
    vector<int>sameElementsPart;
    int temp = 1;

    for(int i=0; i<rowPart.size(); i++)
    {
            if(!(rowPart.at(i)==1)&&!(rowPart.at(i)==temp))
            {
                sameElementsPart.push_back(count(rowPart.begin(),
                rowPart.end(), rowPart.at(i)));

                temp = rowPart.at(i);
            }
    }

    return sameElementsPart;
}

//Calculate the total number of autocorrelations for any power of a Q-vector
//Constrains: k must be even, M >= k
void QvectorNumberAuto(int k, int M)
{
    const int n = k/2;
    int p[n];
    int m = 0;
    p[m] = n; //first: all indices are the same

    //to store a possible partitions combination (p.p.c.)
    vector<int> rowPart;

    //to store how many identical partitions exist in one p.p.c.
    vector<int> sameElementsPart;

    long long int result = 0;
```

```
while (true)
{
    //print partitions
    printArray(p, m+1);

    //safety clear and store current p.p.c.
    rowPart.clear();
    rowPart = storePartitions(p,m+1);

    //safety clear and store number of
    //identical partitions in p.p.c. (excluding 1)
    sameElementsPart.clear();
    sameElementsPart = numberSameEntries(rowPart);

    //calculate add number of autocorrelations in p.p.c.
    result += combinations(k,&rowPart)*permutations(k,
    &rowPart, &sameElementsPart)*variations(rowPart.size(),M);

    // Generate next partition
    int r_val = 0;

    while (m >= 0 && p[m] == 1)
    {
        r_val += p[m];
        m--;
    }

    if (m < 0)
    {
            cout
            <<"Number of autocorrelations for the Q-vector to the power "
            <<k<<" and the multiplicity "<<M<< " is: "<< result<<endl;
            return;
    }

    p[m]--;
    r_val++;

    while (r_val > p[m])
    {
        p[m+1] = p[m];
        r_val = r_val - p[m];
        m++;
    }

    p[m+1] = r_val;
    m++;

}
```

```
}


int main()
{
    //example
    QvectorNumberAuto(8,9);

    return 0;
}
```

B.3.2 Visual representation of autocorrelation in even power $\langle |Q_n|^k \rangle$

The recursiveness and visual representation of how many autocorrelations cases there actually are, can be seen in Fig. B.3 and Fig. B.4. In them, all possible values of the indices for $M = 8$ in the cases $|Q_n|^2$, $|Q_n|^4$ and $|Q_n|^6$ are shown. Since $|Q_n|^4$ and $|Q_n|^6$ would be a 4- or 6-dimensional array, they are simply flattened to 1D and chopped for a square in 2D. Nevertheless, the recursiveness can be seen as Fig. B.3a appears in all possible alterations 8×8-times in Fig. B.3b. Fig. B.3b appears in all possible alterations 8×8-times in Fig. B.4.

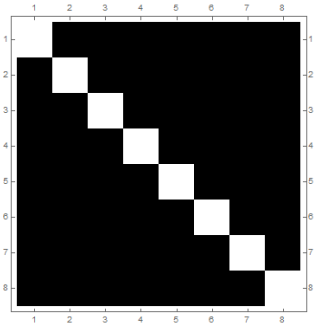

(a) This is the case $|Q_n|^2$

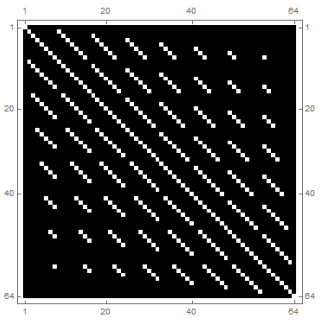

(b) This is the case $|Q_n|^4$

Figure B.3: Visual representation of all possible indices combinations flattened with $M = 8$. White squares are vanishing indices/autocorrelations.

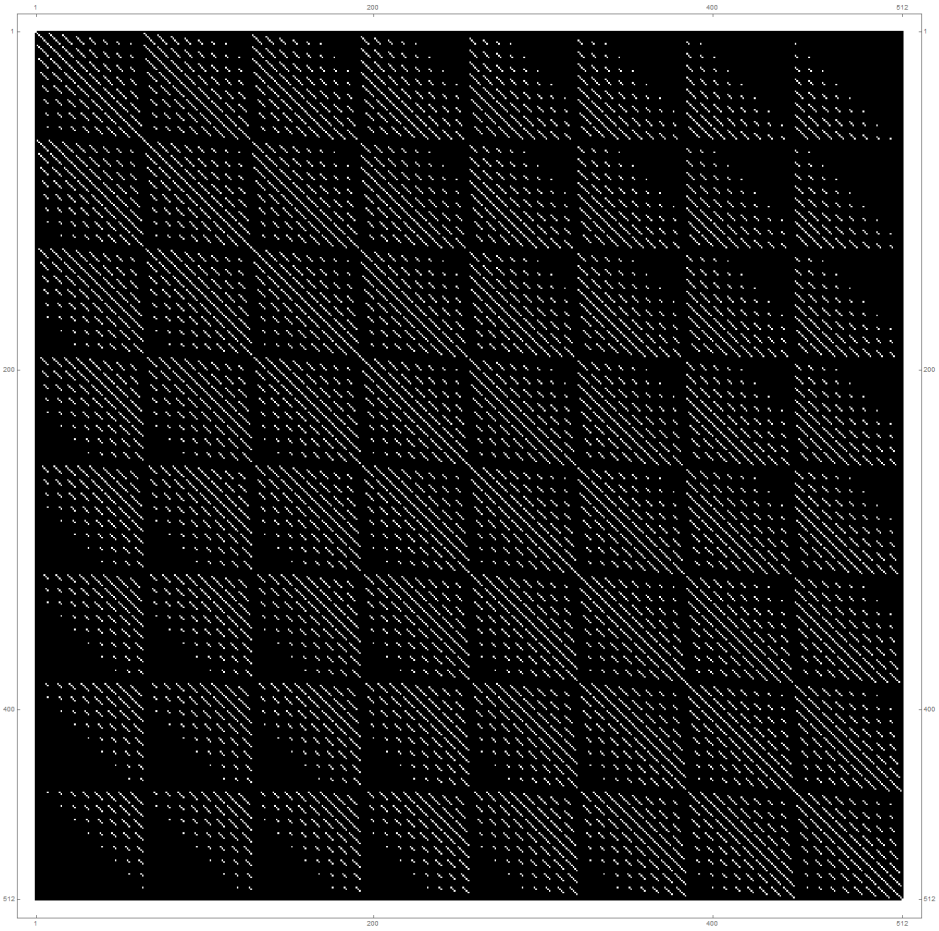

Figure B.4: Visual representation of all possible indices combinations flattened with $M = 8$. White squares are vanishing indices/autocorrelations. This is the case $|Q_n|^8$.

Appendix C

$\langle 6 \rangle = 0$ and $\langle 8 \rangle = 0$

The obtained results for the number of autocorrelations were independently verified via Mathematica [40].

C.1 Case: $\langle 6 \rangle = 0$

Let's first look at the 6-particle correlator:

$$\langle 6 \rangle = \underbrace{\langle \exp[in(\varphi_1 + \varphi_2 + \varphi_3 - \varphi_4 - \varphi_5 - \varphi_6)] \rangle}_{\varphi_1 \neq \varphi_2 \neq \varphi_3 \neq \varphi_4 \neq \varphi_5 \neq \varphi_6} \tag{C.1}$$

$$= \frac{1}{\binom{M}{6} 6!} \times [|Q_n|^6 + 9 \cdot |Q_{2n}|^2 |Q_n|^2 - 6 \cdot \Re[Q_{2n} Q_n Q_n^* Q_n^* Q_n^*] \tag{C.2}$$

$$+ 4 \cdot \Re[Q_{3n} Q_n^* Q_n^* Q_n^*] - 12 \cdot \Re[Q_{3n} Q_{2n}^* Q_n^*] \tag{C.3}$$

$$+ 18(M-4)\Re[Q_{2n} Q_n^* Q_n^*] + 4 \cdot |Q_{3n}|^2 \tag{C.4}$$

$$- 9(M-4)(|Q_n|^4 + |Q_{2n}|^2) + 18(M-2)(M-5)|Q_n|^2 \tag{C.5}$$

$$- 6M(M-4)(M-5)]. \tag{C.6}$$

Let's look at all the occurring Q-vectors and their scaling in the random walk.

C.1.1 $|Q_n|^6$:

$\boxed{1\ 2\ 3}\ | \Rightarrow \mathrm{M}$

$\boxed{1\ 2}\ \textcircled{3}\ | \Rightarrow \frac{1}{2!} 3! \binom{3}{2} M(M-1)$

$\textcircled{1}\ \textcircled{2}\ \textcircled{3}\ | \Rightarrow 3! \frac{M!}{(M-3)!}$

This sums up to:

$$\langle |Q_n|^6 \rangle = M(4 - 9M + 6M^2) + \langle \mathcal{O}(e^{i\Delta\bar{\varphi}}) \rangle. \tag{C.7}$$

C.1.2 $|Q_n|^2$ or $|Q_{2n}|^2$ or $|Q_{3n}|^2$:

$\boxed{1}\,| \Rightarrow$ M
This sums up to:

$$\langle |Q_n|^2 \rangle = M + \langle \mathcal{O}(e^{i\Delta\bar{\varphi}}) \rangle. \tag{C.8}$$

C.1.3 $\Re[Q_{2n}Q_nQ_n^*Q_n^*Q_n^*]$:

$$Q_{2n}Q_nQ_n^*Q_n^*Q_n^* = \sum_{i,j,k,l,m=1}^{M} e^{in(\varphi_i+\varphi_i+\varphi_j-\varphi_k-\varphi_l-\varphi_m)}. \tag{C.9}$$

Here of course two azimuthal angles are *coupled*, since the whole argument has to be isotropic. Let's reduce this and calculate the terms that survive the random walk: $\boxed{1\ 2\ 3}\,|+\boxed{1\ 2}\boxed{3}\,|$ or $\square\square\square + \begin{smallmatrix}\square\square\\ \square\end{smallmatrix}$.

No further partitions are possible due to the coupling. Additionally due to the *coupling*, the choice of the "two same indices" is "forced" and thus $\binom{3}{2}$ can't occur. (We have no option to choose which indices should be the same.) This translates into:

$$\langle Q_{2n}Q_nQ_n^*Q_n^*Q_n^* \rangle = M + \frac{3!}{2!} \cdot M(M-1) + \langle \mathcal{O}(e^{i\Delta\bar{\varphi}}) \rangle \tag{C.10}$$

$$= M(3M-2) + \langle \mathcal{O}(e^{i\Delta\bar{\varphi}}) \rangle. \tag{C.11}$$

Since our result is real we directly get:

$$\langle \Re[Q_{2n}Q_nQ_n^*Q_n^*Q_n^*] \rangle = M(3M-2) + \langle \mathcal{O}(e^{i\Delta\bar{\varphi}}) \rangle. \tag{C.12}$$

C.1.4 $\Re[Q_{3n}Q_n^*Q_n^*Q_n^*]$ and $\Re[Q_{3n}Q_{2n}^*Q_n^*]$ and $\Re[Q_{2n}Q_n^*Q_n^*]$:

Now we have 3 indices coupled $\boxed{1\ 2\ 3}\,| \Rightarrow$ M
This sums up to:

$$\langle \Re[Q_{3n}Q_n^*Q_n^*Q_n^*] \rangle = M + \langle \mathcal{O}(e^{i\Delta\bar{\varphi}}) \rangle. \tag{C.13}$$

Or we have 2 indices coupled $\boxed{1\ 2}\,| \Rightarrow$ M
This sums up to:

$$\langle \Re[Q_{2n}Q_n^*Q_n^*] \rangle = M + \langle \mathcal{O}(e^{i\Delta\bar{\varphi}}) \rangle. \tag{C.14}$$

C.1.5 $\langle |Q_n|^4 \rangle$:

$\boxed{1\ 2}\ | \Rightarrow$ M
$\textcircled{1}\ \textcircled{2}\ | \Rightarrow 2!\frac{M!}{(M-2)!}$
This sums up to:

$$\langle |Q_n|^4 \rangle = M(-1+2M) + \langle \mathcal{O}(e^{i\Delta\bar{\varphi}}) \rangle. \tag{C.15}$$

C.2 Case: $\langle 8\rangle = 0$

Let's first look at the 8-particle correlator

$$\begin{aligned}
\langle 8\rangle = \underbrace{\langle \exp[in(\varphi_1+\varphi_2+\varphi_3+\varphi_4-\varphi_5-\varphi_6-\varphi_7-\varphi_8)]\rangle}_{\varphi_1\neq\varphi_2\neq\varphi_3\neq\varphi_4\neq\varphi_5\neq\varphi_6\neq\varphi_7\neq\varphi_8} \\
= \frac{1}{\binom{M}{6}6!} \times [|Q_n|^8 - 12\cdot Q_{2n}Q_nQ_nQ_n^*Q_n^*Q_n^*Q_n^* \\
+6\cdot Q_{2n}Q_{2n}Q_n^*Q_n^*Q_n^*Q_n^* + 16\cdot Q_{3n}Q_nQ_n^*Q_n^*Q_n^*Q_n^* \\
-96\cdot Q_{3n}Q_nQ_{2n}^*Q_n^*Q_n^* - 12\cdot Q_{4n}Q_n^*Q_n^*Q_n^*Q_n^* \\
-36\cdot Q_{2n}Q_{2n}Q_{2n}^*Q_n^*Q_n^* + 96(M-6)\cdot Q_{2n}Q_nQ_n^*Q_n^*Q_n^* \\
+72\cdot Q_{4n}Q_{2n}^*Q_n^*Q_n^* + 48\cdot Q_{3n}Q_nQ_{2n}^*Q_{2n}^* \\
-64(M-6)\cdot Q_{3n}Q_n^*Q_n^*Q_n^* + 192(M-6)\cdot Q_{3n}Q_{2n}^*Q_n^* \\
-96\cdot Q_{4n}Q_{3n}^*Q_n^* - 36\cdot Q_{4n}Q_{2n}^*Q_{2n}^* \\
-144(M-7)(M-4)Q_{2n}Q_n^*Q_n^* + 36|Q_{4n}|^2 + 64|Q_{3n}|^2|Q_n|^2 \\
-64(M-6)|Q_{3n}|^2 + 9|Q_{2n}|^2 + 36|Q_n|^4|Q_{2n}|^2 \\
-144(M-6)|Q_{2n}|^2|Q_n|^2 \\
+72(M-7)(M-4)(|Q_{2n}|^2+|Q_n|^4) - 16(M-6)|Q_n|^6 \\
96(M-7)(M-6)(M-2)|Q_n|^2 \\
24M(M-7)(M-6)(M-5)].
\end{aligned} \tag{C.16}$$

Here 6 Q-vector combinations appear that we haven't calculated yet. All results have been verified through Mathematica [40].

C.2.1 $Q_{2n}Q_nQ_nQ_n^*Q_n^*Q_n^*$

$\boxed{1\ 2\ 3\ 4}| \Rightarrow$ M
$\boxed{1\ 2\ 3}\textcircled{4}| \Rightarrow \frac{1}{3!}4!\binom{2}{1}M(M-1)$

$\boxed{1\ 2}\textcircled{3}\textcircled{4}| + \boxed{1\ 2}\boxed{3\ 4}| \Rightarrow \frac{1}{2!}4!M(M-1)(M-2) + \frac{1}{2!2!}4!\binom{4-2}{2}M(M-1)$
This sums up to:

$$\langle Q_{2n}Q_nQ_nQ_n^*Q_n^*Q_n^*\rangle = M(11-22M+12M^2) + \langle\mathcal{O}(e^{i\Delta\bar{\varphi}})\rangle. \quad \text{(C.17)}$$

C.2.2 $Q_{2n}Q_{2n}Q_n^*Q_n^*Q_n^*Q_n^*$

$\boxed{1\ 2\ 3\ 4}| \Rightarrow$ M
$\boxed{1\ 2}\boxed{3\ 4}| \Rightarrow \frac{1}{2!2!}4!M(M-1)$
Through the *coupling* some decisions where *forced*. This sums up to:

$$\langle Q_{2n}Q_{2n}Q_n^*Q_n^*Q_n^*Q_n^*\rangle = M(-5+6M) + \langle\mathcal{O}(e^{i\Delta\bar{\varphi}})\rangle. \quad \text{(C.18)}$$

C.2.3 $Q_{3n}Q_nQ_n^*Q_n^*Q_n^*Q_n^*$

$\boxed{1\ 2\ 3\ 4}| \Rightarrow$ M
$\boxed{1\ 2\ 3}\textcircled{4} \Rightarrow \frac{1}{3!}4!M(M-1)$
Through the *coupling* some decisions were *forced*. This sums up to:

$$\langle Q_{3n}Q_nQ_n^*Q_n^*Q_n^*Q_n^*\rangle = M(-3+4M) + \langle\mathcal{O}(e^{i\Delta\bar{\varphi}})\rangle. \quad \text{(C.19)}$$

C.2.4 $Q_{3n}Q_nQ_{2n}^*Q_n^*Q_n^*$

$\boxed{1\ 2\ 3\ 4}\|\boxed{5\ 6\ 7\ 8} \Rightarrow$ M
$\boxed{1\ 2\ 3}\textcircled{4}\|\boxed{5\ 6}\textcircled{7}\textcircled{8} \Rightarrow 2M(M-1)$
Through the *coupling* some decisions were *forced*. This sums up to:

$$\langle Q_{3n}Q_nQ_{2n}^*Q_n^*Q_n^*\rangle = M(-1+2M) + \langle\mathcal{O}(e^{i\Delta\bar{\varphi}})\rangle. \quad \text{(C.20)}$$

C.2.5 $Q_{2n}Q_{2n}Q_{2n}^*Q_n^*Q_n^*$

$\boxed{1\ 2\ 3\ 4}\|\boxed{5\ 6\ 7\ 8} \Rightarrow$ M
$\boxed{1\ 2}\boxed{3\ 4}\|\boxed{5\ 6}\textcircled{7}\textcircled{8} \Rightarrow 2M(M-1)$
Through the *coupling* some decisions were *forced*. This sums up to:

$$\langle Q_{2n}Q_{2n}Q_{2n}^*Q_n^*Q_n^**\rangle = M(-1+2M) + \langle\mathcal{O}(e^{i\Delta\bar{\varphi}})\rangle. \quad \text{(C.21)}$$

C.2.6 $Q_{3n}Q_nQ_{2n}^*Q_{2n}^*$

$\boxed{1\ 2\ 3\ 4}\| \Rightarrow \mathrm{M}$

Through the *coupling* some decisions were *forced*. Summed up this results in:

$$\langle Q_{3n}Q_nQ_{2n}^*Q_{2n}^* \rangle = M + \langle \mathcal{O}(e^{i\Delta\bar{\varphi}}) \rangle. \tag{C.22}$$

Appendix D

Statistical error propagation

D.1 Statistical error propagation in Q-Cumulants

The statistical error of the Q-Cumulants

$$QC\{2\} \equiv \langle\langle 2\rangle\rangle, \tag{D.1}$$
$$QC\{4\} \equiv \langle\langle 4\rangle\rangle - 2 \cdot \langle\langle 2\rangle\rangle^2, \tag{D.2}$$
$$QC\{6\} \equiv \langle\langle 6\rangle\rangle - 9 \cdot \langle\langle 2\rangle\rangle\langle\langle 4\rangle\rangle + 12 \cdot \langle\langle 2\rangle\rangle^3, \tag{D.3}$$
$$\tag{D.4}$$

are given through the Gaussian error propagation:

$$\Delta g = \sqrt{\Delta x^2 [\frac{\partial g}{\partial x}]^2_{\bar{x},\bar{y},\ldots} + \Delta y^2 [\frac{\partial g}{\partial y}]^2_{\bar{x},\bar{y},\ldots} + \ldots.} \tag{D.5}$$

This results in:

$$\Delta QC\{2\} = \Delta\langle\langle 2\rangle\rangle, \tag{D.6}$$
$$\Delta QC\{4\} = \sqrt{(\Delta\langle\langle 4\rangle\rangle)^2 + 16(\Delta\langle\langle 2\rangle\rangle) \cdot (\langle\langle 2\rangle\rangle)^2}, \tag{D.7}$$
$$\Delta QC\{6\} = \sqrt{(\Delta\langle\langle 6\rangle\rangle)^2 + 81 \cdot (\Delta\langle\langle 2\rangle\rangle)^2(\langle\langle 4\rangle\rangle)^2 + (\Delta\langle\langle 2\rangle\rangle)^2)(9 \cdot \langle\langle 4\rangle\rangle - 36 \cdot (\langle\langle 2\rangle\rangle)^2)^2}. \tag{D.8}$$

D.2 Statistical error propagation of $v_n\{2\}$ and $v_n\{4\}$

Applying the Gaussian error propagation to

$$v_n\{2\} = \sqrt{\langle\langle 2\rangle\rangle}, \tag{D.9}$$
$$v_n\{4\} = \sqrt[4]{-c_n\{4\}}, \tag{D.10}$$

it results in

$$\sigma_{v_{n\{2\}}} = \frac{\Delta\langle\langle 2\rangle\rangle}{2\sqrt{\langle\langle 2\rangle\rangle}}, \tag{D.11}$$

$$\sigma_{v_{n\{4\}}} = \frac{\sqrt{16\langle\langle 2\rangle\rangle^2(\Delta\langle\langle 2\rangle\rangle)^2 + (\Delta\langle\langle 4\rangle\rangle)^2}}{4\cdot(2\langle\langle 2\rangle\rangle^2 - \langle\langle 4\rangle\rangle)^{3/4}}. \tag{D.12}$$

Bibliography

[1] J. Collins and M. Perry, "Superdense matter: Neutrons or asymptotically free quarks?," *Physical Review Letters*, vol. 34, pp. 1353–1356, 1 1975.

[2] S. A. Chin, "Transition to Hot Quark Matter in Relativistic Heavy Ion Collision," *Phys. Lett.*, vol. 78B, pp. 552–555, 1978.

[3] D. Teaney, J. Lauret, and E. V. Shuryak, "Flow at the sps and rhic as a quark-gluon plasma signature," *Phys. Rev. Lett.*, vol. 86, pp. 4783–4786, May 2001.

[4] "New state of matter created at cern." `https://home.cern/news/press-release/cern/new-state-matter-created-cern`. Accessed: 2019-07-04.

[5] "Rhic scientists serve up 'perfect' liquid." `https://www.bnl.gov/newsroom/news.php?a=110303`. Accessed: 2019-07-04.

[6] K. t. Aamodt, "Elliptic flow of charged particles in pb-pb collisions at $\sqrt{s_{NN}} = 2.76$ TeV," *Phys. Rev. Lett.*, vol. 105, p. 252302, Dec 2010.

[7] P. Kovtun, D. T. Son, and A. O. Starinets, "Viscosity in strongly interacting quantum field theories from black hole physics," 2004.

[8] H. Niemi, G. S. Denicol, P. Huovinen, E. Molnar, and D. H. Rischke, "Influence of the shear viscosity of the quark-gluon plasma on elliptic flow in ultrarelativistic heavy-ion collisions," 2011.

[9] R. S. Bhalerao, "Relativistic heavy-ion collisions," 2014.

[10] S. Chun, "*Sketch of relativistic heavy-ion collisions*," 2014.

[11] M. L. Miller, K. Reygers, S. J. Sanders, and P. Steinberg, "Glauber modeling in high energy nuclear collisions," 2007.

[12] W. E. B. R. J. Glauber. Interscience. Lecture in Theoretical Physics and V. . p. L. G. Dunham (eds.) New York, 1959

[13] A. Bilandzic, *Anisotropic Flow Measurements in ALICE at the Large Hadron Collider*. Utrecht University, 2012.

[14] R. Snellings, "Collective Expansion at the LHC: selected ALICE anisotropic flow measurements," *J. Phys.*, vol. G41, no. 12, p. 124007, 2014.

[15] C. Lefèvre, "The CERN accelerator complex. Complexe des accélérateurs du CERN." Dec 2008.

[16] "LHC the guide." `http://cds.cern.ch/record/2255762/files/CERN-Brochure-2017-002-Eng.pdf`. Accessed: 2019-07-04.

[17] T. A. Collaboration, "Observation of a new particle in the search for the standard model higgs boson with the atlas detector at the lhc," 2012.

[18] T. C. Collaboration, "Observation of a new boson at a mass of 125 gev with the cms experiment at the lhc," 2012.

[19] A. Collaboration, "Performance of the alice experiment at the cern lhc," 2014.

[20] T. A. Collaboration and K. A. *et al.*, "The ALICE experiment at the CERN LHC," *Journal of Instrumentation*, vol. 3, pp. S08002–S08002, aug 2008.

[21] A. Collaboration, "Alignment of the alice inner tracking system with cosmic-ray tracks," 2010.

[22] G. Dellacasa *et al.*, "ALICE: Technical design report of the time projection chamber," 2000.

[23] G. Dellacasa *et al.*, "ALICE technical design report of the inner tracking system (ITS)," 1999.

[24] A. T. for the ALICE Collaboration, "Bulk properties of pb-pb collisions at sqrt(snn) = 2.76 tev measured by alice," 2011.

[25] P. Cortese *et al.*, "ALICE technical design report on forward detectors: FMD, T0 and V0," 2004.

[26] M. Miller and R. Snellings, "Eccentricity fluctuations and its possible effect on elliptic flow measurements," 2003.

[27] R. Snellings, "Elliptic flow: A brief review," 2011.

[28] S. Voloshin and Y. Zhang, "Flow study in relativistic nuclear collisions by fourier expansion of azimuthal particle distributions," 1994.

[29] A. Puglisi, *Transport coefficients and early time dynamics of the Quark-Gluon Plasma created in ultra-relativistic heavy ion collisions.* PhD thesis, Catania U., 2016-02-20.

[30] R. S. Bhalerao, M. Luzum, and J.-Y. Ollitrault, "Determining initial-state fluctuations from flow measurements in heavy-ion collisions," 2011.

[31] P. Gavriliadis, "Moment information for probability distributions, without solving the moment problem. i: Where is the mode?," *Communications in Statistics-theory and Methods - COMMUN STATIST-THEOR METHOD*, vol. 37, pp. 671–681, 01 2008.

[32] A. Bilandzic, C. H. Christensen, K. Gulbrandsen, A. Hansen, and Y. Zhou, "Generic framework for anisotropic flow analyses with multiparticle azimuthal correlations," 2013.

[33] N. Borghini, P. M. Dinh, and J. Y. Ollitrault, "Analysis of directed flow from elliptic flow," 2002.

[34] N. Borghini, P. M. Dinh, and J.-Y. Ollitrault, "New method for measuring azimuthal distributions in nucleus-nucleus collisions," 2000.

[35] R. Kubo, "Generalized cumulant expansion method," *Journal of the Physical Society of Japan*, vol. 17, no. 7, pp. 1100–1120, 1962.

[36] A. Collaboration, "Elliptic flow of charged particles in pb-pb collisions at 2.76 tev," 2010.

[37] P. D. Francesco, M. Guilbaud, M. Luzum, and J.-Y. Ollitrault, "Systematic procedure for analyzing cumulants at any order," 2016.

[38] G. Andrews, *The theory of partitions*, p. 69. Cambridge New York, NY, USA: Cambridge University Press, 1998.

[39] F. Schwabl, *Statistische Mechanik : mit 26 Tabellen und 186 Aufgaben*, p. 9. Berlin: Springer, 2006.

[40] W. R. Inc., "Mathematica, Version 12.0." Champaign, IL, 2019.

Acknowledgement

I would like to thank my supervisor Ante Bilandžić for teaching me all necessary skills. Furthermore, I would like to thank him and Marcel Lesch for always being helpful in battling bugs.